A mathematical investigation of the effects of inhibitor therapy on three putative phosphorylation cascades governing the two-component system of the agr operon

Jabbari, Sara; King, John R; Williams, Paul

DOI:
10.1016/j.mbs.2010.03.001

Document Version
Peer reviewed version

Citation for published version (Harvard):
Jabbari, S, King, JR & Williams, P 2010, 'A mathematical investigation of the effects of inhibitor therapy on three putative phosphorylation cascades governing the two-component system of the agr operon', *Mathematical biosciences*, vol. 225, no. 2, pp. 115-31. https://doi.org/10.1016/j.mbs.2010.03.001

A mathematical investigation of the effects of inhibitor therapy on three putative phosphorylation cascades governing the two-component system of the *agr* operon

Sara Jabbari*, John R. King

School of Mathematical Sciences, University of Nottingham, Nottingham, NG7 2RD, UK

**Corresponding author. Email: sara.jabbari@nottingham.ac.uk*

Paul Williams

Centre for Biomolecular Sciences, University of Nottingham, Nottingham, NG7 2RD, UK

The final published article is available at http://www.sciencedirect.com/science/article/pii/S0025556410000362

Abstract

Two-component systems (TCSs) are widely employed by bacteria to sense specific external signals and conduct an appropriate response via a phosphorylation cascade within the cell. The TCS of the *agr* operon in the bacterium *Staphylococcus aureus* forms part of a regulatory process termed quorum sensing, a cell-to-cell communication mechanism used to assess population density. Since *S. aureus* manipulates this "knowledge" in order to co-ordinate production of its armoury of exotoxin virulence factors required to promote infection, it is important to understand fully how this process works. We present three models of the *agr* operon, each incorporating a different phosphorylation cascade for the TCS since the precise nature of the cascade is not fully understood. Using numerical and asymptotic techniques we examine the effects of inhibitor therapy, a novel approach to controlling bacterial infection through the attenuation of virulence, on each of these three cascades. We present results which, if evaluated against appropriate experimental data, provide insights into the potential effectiveness of such therapy. Moreover, the TCS models presented here are of broad relevance given that TCSs are widely conserved throughout the bacterial kingdom.

Keywords: two component systems, quorum sensing, *Staphylococcus aureus*, mathematical modelling, asymptotic analysis.

1 Introduction

A two-component system (TCS) is a signal-transduction mechanism used by bacteria as a means of detecting and eliciting an appropriate response to an external signal [1]. This signal could be, for example, temperature, pH or (in the case of the *agr* operon of *Staphylococcus aureus*) the bacterial population density, as monitored via a self-generated signal molecule. A TCS comprises a sensor/receptor protein in the membrane of the cell and a response regulator within the cell cytoplasm. The receptor recognises a specific external cue and transfers this "knowledge" to the response regulator via a phosphorylation cascade, thus allowing the cytoplasmic protein to provoke some appropriate response from the cell, usually a change in gene expression which will facilitate adaptation of the bacterium to the specific environmental challenge.

The activation cascade can vary between TCSs (for a review, see [2]). In a classical TCS, detection of the signal by the receptor protein results in autophosphorylation followed by the transfer of the phosphate to the response regulator protein. When gene expression is the ultimate target, the phosphorylated protein usually has a higher affinity for the relevant DNA binding site than when in the un-phosphorylated state. This phosphorylation cascade can vary between TCSs and we shall investigate the implications of the possibility that the TCS of the *agr* operon might not take this conventional form.

The *agr* operon was first discovered in the Gram-positive bacteria *S. aureus* [3] and, as mentioned above, is a cell-to-cell communication device which is generally considered to facilitate the co-ordination of gene expression at the population level rather than individual cell level. Cell-to-cell communication in bacteria is usually called quorum sensing (QS) and is used by *S. aureus* in order to, amongst other things, control the production of virulence factors during infection. While its population size is small, *S. aureus* produces surface proteins which facilitate adherence to host tissue and aid immune evasion. As the population grows, a switch to the production of secreted virulence factors occurs, leading to the damage and degradation of the surrounding host cells and tissues, thus actively attacking the host. Since tissue damage will alert host defence systems, such a delayed 'deployment tactic' may allow the infecting bacteria time to reach a sufficient population size to be able to overwhelm the host [4]. The sequencing of large numbers of bacterial genomes has revealed that *agr*-type QS systems are conserved in many more Gram-positive bacterial species, including the pathogens *Clostridium botulinum* [5], *Clostridium perfringens* [6], *Enterococcus faecelis* [7] and *Listeria monocytogenes* [8]. Thus, while the implications of this study are discussed principally in relation to *S. aureus*, the results are more widely relevant.

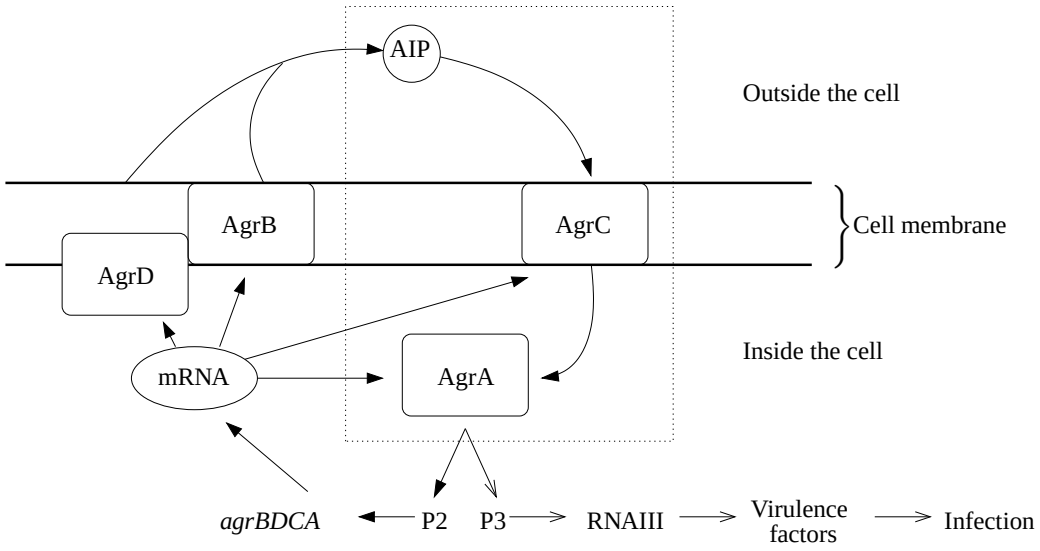

Figure 1: A schematic representation of the *agr* feedback loop in *S. aureus*. The arrows with a filled head illustrate the positive feedback loop. The dotted box encloses the elements of the TCS.

In *S. aureus*, the operon consists of two transcription units, termed *agrBDCA* and RNAIII (for reviews see [9] or [10]). These are driven by regulatory proteins which bind to promoters termed P2 and P3, thereby permitting RNA polymerase to transcribe the DNA into mRNA prior to translation of *agr* mRNA into proteins at the ribosomes. The P2 transcript consists of four genes that are transcribed and translated to give the four proteins AgrB, AgrD, AgrC and AgrA. AgrB is a transmembrane protein and is involved in the post-translational conversion of the membrane-anchored AgrD pro-peptide into a cyclic peptide QS signal molecule termed an autoinducing peptide (AIP). The AIP is secreted into the external environment of the cell [11] where it is sensed by the transmembrane AgrC protein which acts as the receptor of the TCS by binding to free AIP molecules [12]. This is an effective method of estimating population size or density since bacterial numbers will, to a certain extent, correlate with the level of AIP molecules in the immediate environment of the *S. aureus* cells. Bound AgrC then activates AgrA, the response regulator [9], via a phosphorylation cascade. Activated AgrA has a higher affinity than non-activated AgrA for the DNA binding sites situated at the two promoters P2 and P3. The P2 promoter controls the *agr* genes, so a positive feedback loop, see Figure 1, is created. The P3 transcript is a regulatory RNA termed RNAIII [13] which directs the increased translation of secreted virulence factors and repression of surface protein production [14]. The presence of enough activated AgrA thus leads to a switch in the behaviour of the population, from what we will call a down-regulated state to an up-regulated one. In other bacteria, the *agr* operon largely takes on this form, though the specific *agr*-induced responses differ.

The emergence of multi-antibiotic resistant *S. aureus* (including methicillin- and vancomycin-resistant *S. aureus*;

MRSA and VRSA respectively), enterococci and *Clostridium difficile* means that understanding the virulence mechanisms employed by these pathogens to cause diseases should aid the development of novel therapies to combat infection through attenuation of virulence. This may be achieved either through the prevention of virulence factor action or by blocking virulence factor production. With respect to the latter, the inhibition of QS offers one potential therapeutic strategy which is already evident in *S. aureus* since some strains were found to interfere with QS in others, a process sometimes referred to as quorum quenching. This is because within the staphylococci, *agr* polymorphisms occur; *S. aureus* has four different specificity groups with distinct AIPs and AgrC sensor domains and cross group AIP-AgrC interactions are inhibitory. Furthermore, intra-group activation and inter-group inhibition are both mediated exclusively by the same group-specific AgrC receptor [5, 6]. Thus while the AIPs from different *S. aureus* groups are sufficiently similar that they will bind to the AgrC receptor proteins of any other strain, they cannot activate the sensor protein and so block activation by the endogenous AIP. Thus intracellular AgrA will not become activated so effectively blocking the QS loop and forcing the fells into, or maintaining them in, a down-regulated state. *Staphylococcus epidermidis* also employs an *agr* operon in its regulation of virulence factor production [15] and it is demonstrated in [16] that its AIP is a potent inhibitor of the *agr* systems of three of the *S. aureus* groups and, conversely, AIP-4 inhibits that of *S. epidermidis*, suggesting that AIP-4 may have evolved to compete with *S. epidermidis*. We include in our model an inhibitor therapy which capitalises on this natural cross-inhibition by *S. aureus*: synthetic inhibitor molecules have been designed to block the QS loop of any strain of *S. aureus* [17], thus downregulating them and potentially providing the immune system with a greater chance of eradicating the bacteria (see [18] or [19] for reviews of this concept). Experimental work has confirmed the potential success of this approach - see for example [20], where a murine *S. aureus* skin abscess infection caused by a strain producing AIP-1 could be prevented by coadministering AIP-2. Since the therapy would not directly kill the bacteria, the chance of resistance developing is greatly reduced in comparison with antibiotic treatment.

While much work has been done on defining the molecular basis by which the *agr* system operates, a question mark remains over the mechanisms governing the TCS in all strains and species that use *agr*. Although it is clear which proteins play the role of receptor and response regulator, it is not always evident how the phosphorylation cascade occurs; in [21], the phosphorylation cascade of the *agr* operon has been highlighted as one of the important open questions requiring investigation before the QS system can be fully exploited for therapeutic gain. In a classical TCS, AgrC would autophosphorylate on binding to an AIP molecule and then transfer this phosphate to AgrA, making the phosphorylated form of this protein the activator of the system. It has recently been shown in laboratory derivatives of *S. aureus*, that AgrC does indeed autophosphorylate [22], implying that in this case, it is a classical TCS in operation. However, given the variety of TCSs in existence [2], suggestions that both AgrA and AgrC could be phosphorylated constitutively in [9]

and evidence that AgrA can bind the relevant DNA binding site in either its phosphorylated or unphosphorylated forms (though it has a higher affinity in the former case) in [23] open up the possibility that the phosphorylation cascade may vary within and between strains depending on the nature of the TCS. Given the ease of testing different hypotheses with mathematical models, as compared with experimental work and, given the prevalence of similar TCSs performing a variety of roles in different bacteria, we investigate in some detail three possibilities for the phosphorylation cascade:

I the *agr* operon employs a classical TCS;

II AgrA is constitutively phosphorylated (so in this case dephosphorylated AgrA is the activator which binds to the DNA);

III transmembrane AgrC is constitutively phosphorylated (and phosphorylated AgrA is the activator which binds to the DNA).

We examine the effect of inhibition with synthetic antagonists on the QS systems governed by each of these three scenarios, presenting time-dependent numerical solutions and bifurcation diagrams showing the response to changes in inhibitor therapy dosage for each of the three models. We are thus able to make comparisons between the three cascade mechanisms, demonstrating that the model assuming AgrA to be constitutively phosphorylated (Model II) is the most sensitive to inhibitor therapy, followed by Model III (which assumes transmembrane AgrC to be phosphorylated in the absence of AIP molecules), with the classical TCS cascade being the most robust. Additionally, we give asymptotic approximations to the steady-state solutions in order to clarify which reactions govern the behaviour of the cells in both the down-regulated and up-regulated states, to give analytical expressions for the threshold levels of inhibitor and to highlight simplified models which could be used for further analysis. These results provide a characterisation of when inhibitor therapy may be successful if the phosphorylation cascade is known; conversely, given suitable experimental data, they may aid the identification of which phosphorylation cascade is dominant in a given strain or species.

2 Model formulation

This work is an extension of our previous model in [24], which treated the entire *agr* operon in the absence of inhibitor molecules. We performed a time-dependent asymptotic analysis on the model, focusing on the feedback loop, in order to investigate the roles of the various interactions which make up the QS system and monitor how a population of *S. aureus* may shift from a relatively harmless state to a highly virulent one. To our knowledge, the only other mathematical model of the *agr* operon is [25] (also focusing on *S. aureus*) which isolates the TCS (taken to be of the classical form) and examines the effect of SarA, another protein involved in the regulation of virulence factors, on the TCS. In the interests

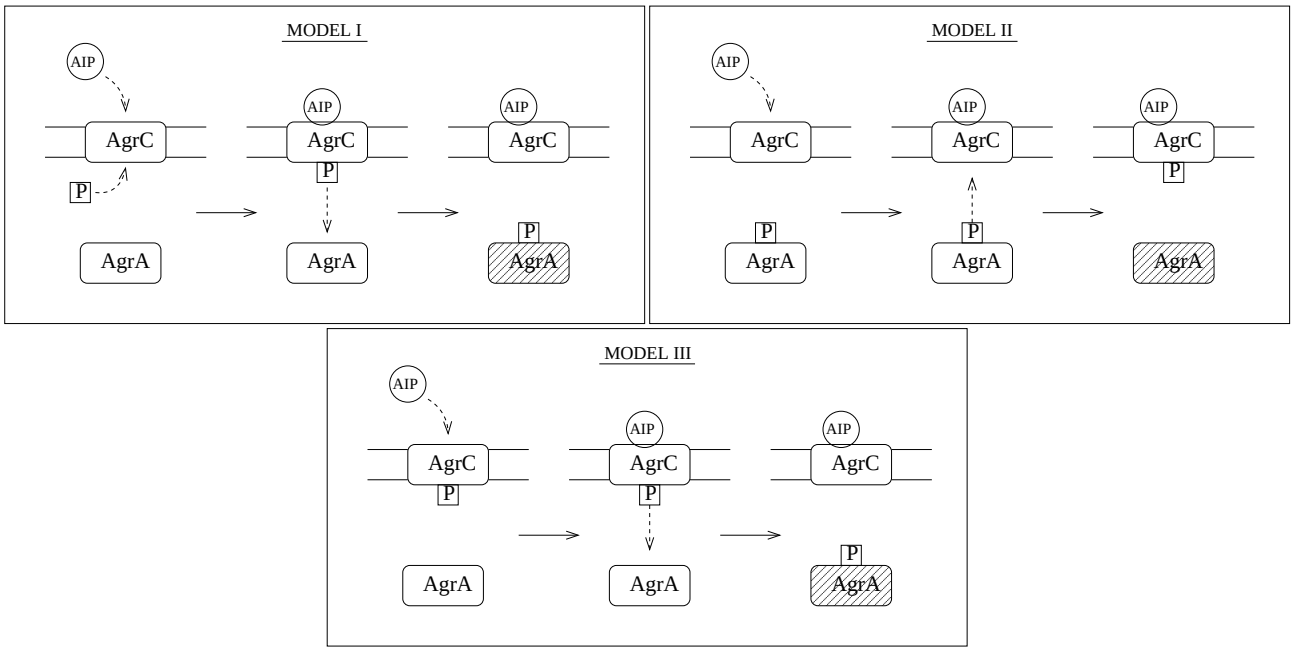

Figure 2: A schematic representation of three different possibilities for the phosphorylation cascade of the TCS of the *agr* operon (the small square represents a phosphate and the activated form of AgrA is in each case shown shaded). Model I follows the classical TCS, as described in §1. Model II allows for the possibility that AgrA is constitutively phosphorylated and consequently it is dephosphorylated AgrA which takes on the role of activator of the *agr* operon. Model III assumes that transmembrane AgrC is phosphorylated in the absence of AIP - upon binding to an AIP molecule it transfers this phosphate to the AgrA protein.

of brevity, we do not provide the full details of the derivation of the formulations of our three models in this paper (they can be found in both [24] and [26], the latter also containing further details of what follows). We instead focus on the assumptions required to differentiate between the three models. Figure 2 illustrates the different phosphorylation cascades and the following is a summary of the differences.

- Model I

  In the case of a classical TCS, once a receptor has bound to an AIP molecule (at a rate β) it can autophosphorylate. To simplify the system we will assume that this process is sufficiently fast that it in effect happens as soon as the receptor binds to the AIP molecule. When the receptor transfers its phosphate to the AgrA protein (at a rate ϕ) it is free to autophosphorylate again, and the phosphorylated AgrA is able to bind to the promoter site of the DNA and upregulate mRNA transcription.

- Model II

  AgrA is phosphorylated constitutively by kinases at a rate ψ_A. We assume that when an AIP molecule binds to a receptor, the latter phosphorylates by removing the phosphate from AgrA (again, we assume that this occurs sufficiently fast that it effectively happens as soon as the receptor binds to the AIP), and this dephosphorylated AgrA is then free to bind to the promoter site of the DNA. We assume that the receptor can obtain a phosphate only from AgrA and not from any other source within the cell; this is required to isolate the TCS from influences outside of the *agr* loop and would reflect specificity of the protein structure.

- Model III

  Model III assumes that once AgrC has become transmembrane it can autophosphorylate at a rate ψ_R. Only when it is bound to an AIP molecule can it transfer this phosphate to an AgrA protein, and only phosphorylated AgrC is able to bind to AIP or to inhibitor molecules. Dephosphorylated AgrC cannot re-phosphorylate while still bound to an AIP molecule. We therefore need to distinguish between AIP-bound phosphorylated and dephosphorylated receptors, as well as unbound phosphorylated and non-phosphorylated receptors, and so extra variables are required for this third scenario. (In Models I and II, receptors are able to re-phosphorylate while still bound to an AIP molecule so these additional variables are not required.) We assume that housekeeping dephosphorylation of transmembrane AgrC is not required since it will not directly affect the level of activator (phosphorylated AgrA) in the cells: if a cell has reached an active state, but then all the AIP is washed away from the cell's environment, housekeeping dephosphorylation of AgrA will aid restoration of the cell to an inactive state; however, housekeeping dephosphorylation of transmembrane AgrC would not alter activator level once AIP is no longer present.

In all the models we assume that AIP- and inhibitor-bound receptors can spontaneously separate [27], at rates γ and γ_i respectively and that AgrA is subject to housekeeping dephosphorylation. We assume that proteins are present at a large enough level to make a continuous approximation appropriate and that the population is well-mixed, so that spatial effects can be neglected. Mass-action expressions are used for all the reaction kinetics - these equations are, for conciseness, shown only in Figures 3, 4 and 5; see Tables 1 and 2 for definitions of variables and parameters and Appendix A for the default initial conditions (these being the naturally down-regulated steady states of the system in the absence of inhibitor molecules; in §3 we also use the initial conditions near the unstable steady state of the full systems in order to examine their bistability).

Variable	Concentration of	Units
M	mRNA	molecules cm^{-3}
A, B, C, D	cytoplasmic AgrA, AgrB, AgrC, AgrD	molecules cm^{-3}
T, R	transmembrane AgrB, AgrC	molecules cm^{-3}
S	anchored AgrD	molecules cm^{-3}
a	free AIP	molecules cm^{-3}
i	free inhibitor	molecules cm^{-3}
R_P^*, R^i	AIP, inhibitor-bound receptor	molecules cm^{-3}
A_P	phosphorylated AgrA	molecules cm^{-3}
P	proportion of cells that is up-regulated i.e. in which the *agr* promoter is bound	-
Model III only variables	Concentration of	Units
R_P	phosphorylated receptor (transmembrane AgrC)	molecules cm^{-3}
R_P^i	inhibitor-bound phosphorylated receptor	molecules cm^{-3}
R^*	AIP-bound dephosphorylated receptor	molecules cm^{-3}

Table 1: Definitions of the variables. Note the slight change of notation from [24]: AIP-bound receptor in its phosphorylated form is denoted R_P^* in this work rather than simply R^*.

We do not consider the possibility that both AgrA and AgrC are constitutively phosphorylated as there would then be no phosphate transfer between the two, meaning that there could be no signal transduction. The three models presented here thus complete the possibilities for the TCS, allowing for a thorough investigation of the different cases.

Whilst most equations follow directly from conventional kinetic theory, that describing the proportion of up-regulated cells is less intuitive and for this we adopt a standard approach used in modelling gene regulation, see for example [28]. Assuming that the activator protein can bind to, and subsequently separate from, a promoter site, the rate of change of the probability that a promoter site is bound (for our purposes this is equivalent to the proportion of *agr* up-regulated cells) is given by

$$\frac{dP}{dt} = \frac{b}{N} A_P (1 - P) - uP, \tag{1}$$

Parameter	Rate constant for	Units
m	basal production of mRNA	molecules cells^{-1} s^{-1}
v	QS-induced mRNA transcription	molecules cells^{-1} s^{-1}
κ	protein translation	s^{-1}
α_T, α_R	AgrB and AgrC taken up into cell membrane	s^{-1}
α_S	AgrD anchoring to cell membrane	s^{-1}
λ_X	natural degradation of variable X	s^{-1}
r	dilution through cell division	s^{-1}
δ_X	degradation and dilution ($\delta_X = \lambda_X + r$)	s^{-1}
k	AIP production from AgrD, mediated by AgrB	molecules^{-1} cm^3 s^{-1}
k_i	introduction of inhibitor into the system	molecules cm^{-3} s^{-1}
β, β_i	binding of AIP, inhibitor to the receptor	molecules^{-1} cm^3 s^{-1}
γ, γ_i	separation of AIP, inhibitor from the receptor	s^{-1}
ϕ	activation of AgrA by AIP-bound AgrC	molecules^{-1} cm^3 s^{-1}
μ	dephosphorylation of AgrA by phosphatases	s^{-1}
b	binding of the promoter site	molecules^{-1} cells s^{-1}
u	unbinding of the promoter site	s^{-1}
ψ_A	AgrA phosphorylation on production (Model II only)	s^{-1}
ψ_R	AIP-independent phosphorylation of transmembrane AgrC (Model III only)	s^{-1}
N	total number of bacteria per unit volume	cells cm^{-3}

Table 2: Definitions of the parameters.

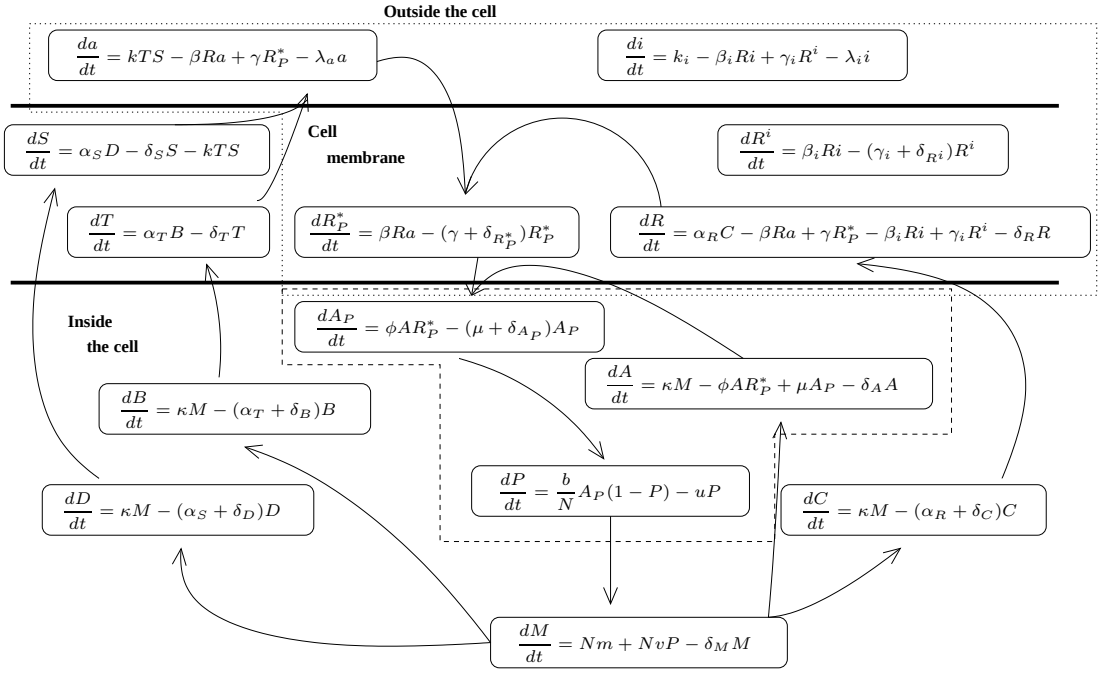

Figure 3: A schematic representation of the complete model for the *agr* circuit with a classical TCS, i.e. Model I with synthetic inhibition. See Tables 1 and 2 for definitions of the variables and parameters. The dimensionless version of this model is shown in Figure 6. The dashed and dotted boxes contain respectively the equations which change for Model II and for Model III. The arrows illustrate the direction of the positive feedback loop.

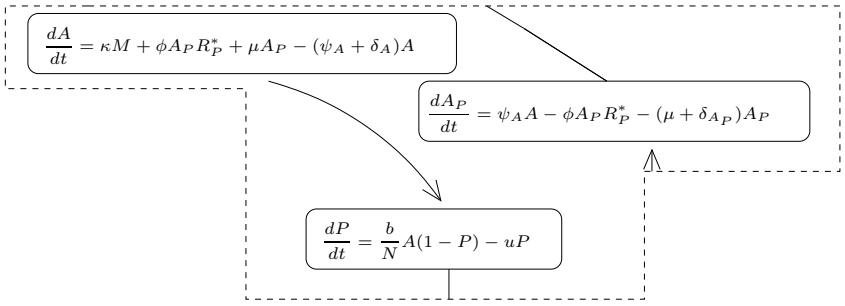

Figure 4: A schematic representation of the section of the model for the *agr* circuit with synthetic inhibition which changes from Model I for Model II. See Tables 1 and 2 for definitions of variables and parameters and Figure 7 for the dimensionless version.

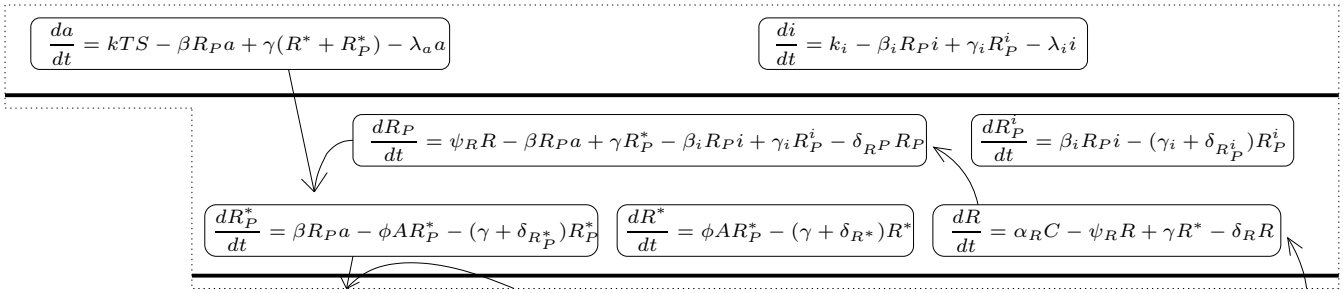

Figure 5: A schematic representation of the section of the model for the *agr* circuit with synthetic inhibition which changes from Model I for Model III. See Tables 1 and 2 for the definitions of variables and parameters and Figure 8 for the dimensionless version.

for Models I and III, and

$$\frac{dP}{dt} = \frac{b}{N} A(1 - P) - uP, \tag{2}$$

for Model II, wherein the activator concentration (molecules per unit volume) is scaled with the population size (number of cells per unit volume), N, in order to obtain the average number of molecules of activator per cell: we assume the proportion of cells which is *agr* up-regulated to be dependent upon this rate. Notice that taking (1) or (2) to be quasi-steady would simply give Michaelis-Menten kinetics for mRNA transcription.

We employ the same nondimensionalisations for Models I and II in order to make comparisons easy, but due to the extra variables in Model III this is not possible. Instead, the nondimensionalisation of Model III is chosen to ensure equivalent terms in Model II have coefficient unity as in Models I and II. The nondimensional systems are shown in Figures 6, 7 and 8. In brief, the steady states of the system are not obtainable explicitly, so we nondimensionalise those variables that would be present in a completely down-regulated cell (one where AIP production is turned off and no inhibitor is present) by their down-regulated steady states. The remaining nondimensionalisations are chosen to simplify the equations as much as possible, namely to set the coefficients of basal mRNA transcription, AIP-receptor binding, AgrA activation and phosphorylated AgrA binding to the promoter site in certain equations to unity. Details are provided in Appendix A and further information can be found in [24] and [26].

As discussed in [24], we do not have sufficient data for full parametrisation of the models. However, we do have enough information to estimate their relative sizes and, given the qualitative nature of our investigations, this is sufficient. We here list our parameter scalings, but more details can be found in [24, 26] (we remark that certain definitions of nondimensional parameters differ in [24], notably η, k_S, ϕ and k_a, with k_i and β_i being new parameters introduced in this study, making the equations superficially different whilst essentially being the same; this is largely due to a minor

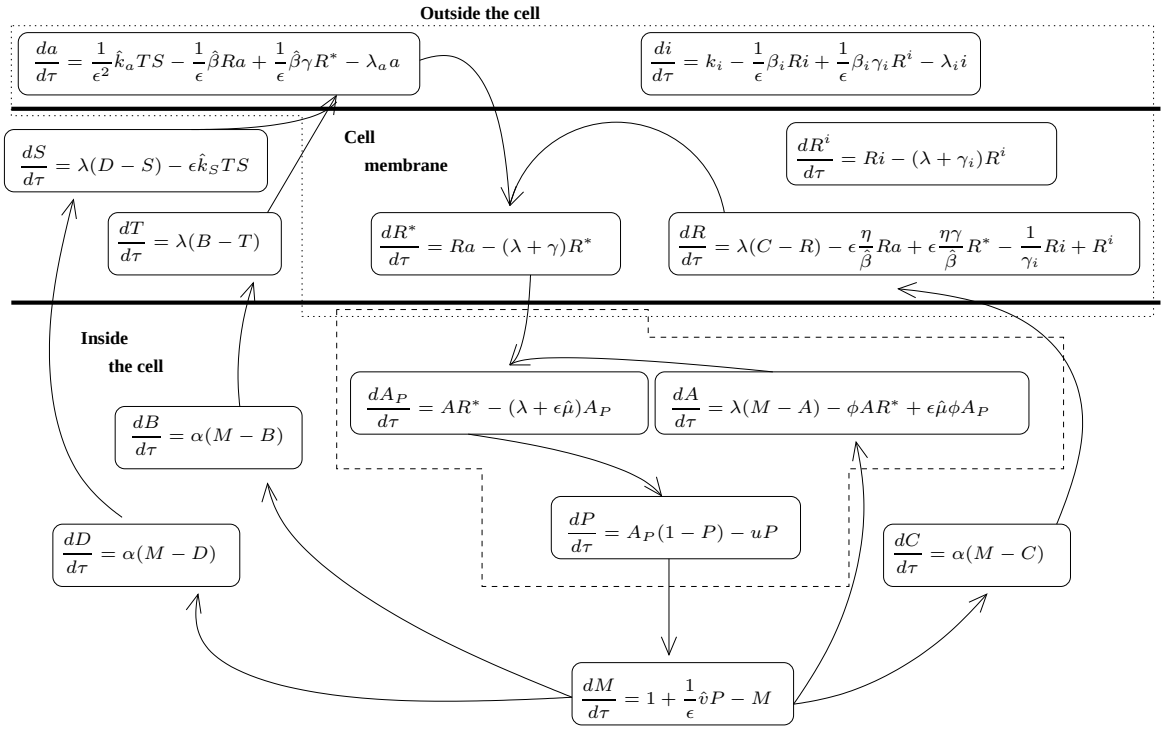

Figure 6: A schematic representation of the nondimensional model of the *agr* circuit incorporating a classical TCS (Model I) with synthetic inhibition. For details of the nondimensionalisation, see Appendix A. We have scaled the parameters according to (4),(5) and (7). The dashed and dotted boxes contain respectively the equations which change for Model II and for Model III.

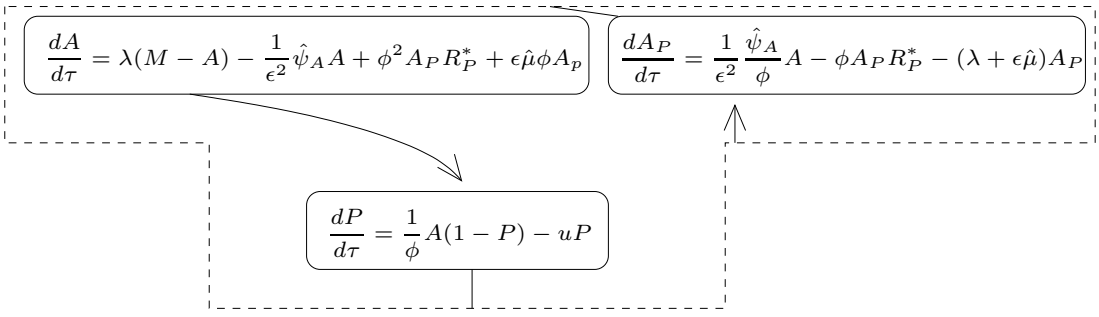

Figure 7: A schematic representation of the section of the nondimensional model of the *agr* circuit with synthetic inhibition which changes from Model I for the Model II TCS. We have scaled the parameters according to (4),(5) and (7).

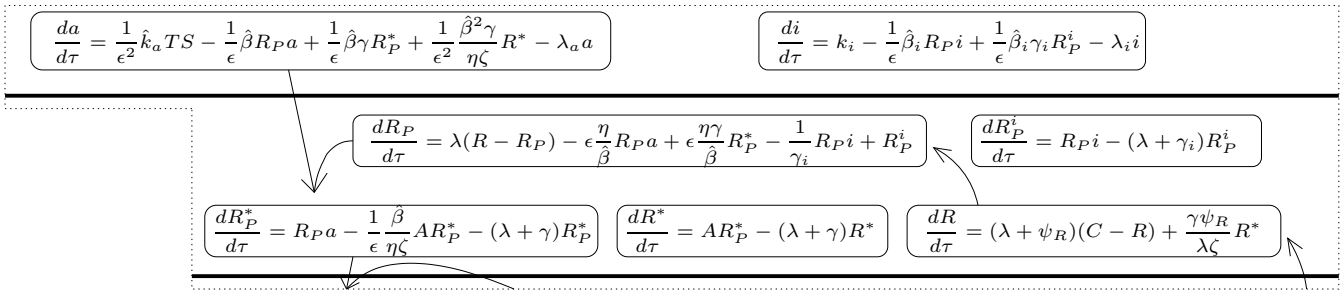

Figure 8: A schematic representation of the section of the nondimensional model of the *agr* circuit with synthetic inhibition which changes from Model I for Model III. We have scaled the parameters according to (4),(5) and (7).

alteration in the parameter scalings, namely that of k_S, which is outlined below). We set ourselves up to apply asymptotic techniques by estimating relative sizes of the nondimensional parameters, our overall parameter choice being motivated by a desire to ensure that the mathematical analysis be revealing as well as biologically plausible. For instance, fundamental to our parameter choice is the ratio of basal transcription to QS-controlled transcription (m/v). To ensure that the cells can 'switch' between an up-regulated and down-regulated state, rather than this transformation being gradual (which would be contrary to the concept of a quorum), this ratio must be small. We thus define our basic small parameter as

$$\epsilon \equiv \frac{m}{v}, \tag{3}$$

where $\epsilon << 1$ (this is consistent with previously published models of QS, for example [29–31]), and scale

$$v' = \frac{1}{\epsilon}\hat{v}, \quad \beta' = \frac{1}{\epsilon}\hat{\beta}, \quad \beta_i' = \frac{1}{\epsilon}\hat{\beta}_i. \tag{4}$$

The first follows directly from (3) while the latter two stem from the assumption that signal binding to receptors is fast in comparison to basal transcription and degradation or translation of proteins (see the nondimensional definitions of these parameters given by (29) in Appendix A). We remark that smaller choices of v' result in the bacteria being unable to achieve a fully up-regulated state even in the absence of inhibitor, while choosing β' this large enables a rapid switch between active and inactive states [24].

We choose our largest parameters to be the rates of AIP production and constitutive AgrA phosphorylation:

$$k_a = \frac{1}{\epsilon^2}\hat{k}_a \quad \text{and} \quad \psi_A = \frac{1}{\epsilon^2}\hat{\psi}_A. \tag{5}$$

The scaling for k_a follows from examination of the dimensional parameters which form k_a:

$$k_a = \frac{k\beta\phi b\tilde{A}\tilde{T}\tilde{R}\tilde{S}}{N{\delta_M}^4}, \tag{6}$$

($\tilde{X}$ is the initial condition of X given by (22), for $X = A, T, R, S$) where we see that k_a has a higher ratio of rates of activation to those of degradation and basal transcription than either v', β' or β_i' and it is therefore logical to take k_a to be larger than either of these three nondimensional parameters. Choosing k_a to be $O(\epsilon^{-2})$ also ensures that, at all times and regardless of how active the cells are initially, enough AIP will be produced (in the absence of any QS inhibition) to upregulate the cells if it is retained within their environment. Constitutive AgrA phosphorylation appears only in Model II and is chosen to be $O(\epsilon^{-2})$ to ensure that that there is not enough activator present in the absence of AIP for the cells to be activated. Additionally, this scaling ensures that Model II displays bistability: a number of the QS systems previously studied demonstrate bistable behaviour (see [25, 30, 32] for example), whereby in a certain parameter regime whether the cells reach an up-regulated or a down-regulated state depends upon the initial conditions. Choosing ψ_A to be $O(\epsilon^{-2})$ results in such bistable behaviour. Hence, both mathematically and biologically, it is logical to choose ψ_A to be large.

Finally, we choose two of the nondimensional parameters to be $O(\epsilon)$. These are

$$\mu' = \epsilon\hat{\mu}, \quad \text{and} \quad k_S = \epsilon\hat{k}_S. \tag{7}$$

The first represents the rate of housekeeping dephosphorylation of AgrA and we assume that the bacteria can eliminate unwanted phosphorylated AgrA via degradation and dilution sufficiently efficiently to make little of this housekeeping process required. In [24] we used $k_S = O(1)$ in order to simplify the asymptotics; however, we here return to the biologically-motivated scaling employed in [26]. The implication of k_S being $O(\epsilon)$ is that AgrD is rapidly turned over in the production of AIPs and reflects the efficiency of the signalling system.

For the timebeing, we leave k_i, the source of inhibitor molecules (corresponding to their entry into the environment of the cells) as $O(1)$. We will investigate how large this parameter must be to make synthetic inhibitor therapy effective for each of the three models. Unless otherwise stated, all dimensionless parameters in our numerical solutions (except ϵ) will be taken to be unity, with $\epsilon = 10^{-2}$. Table 3 displays the default parameter set with the scaled parameters displayed in their non-hatted form in order to be able to see their relative magnitudes. In [24, 26] we were able to demonstrate through a time-dependent asymptotic analysis that for this parameter choice, each of the reactions involved in upregulating the *agr* operon will appear in the leading-order behaviour of the system in the sequence expected from biological knowledge. Thus the parameters are biologically realistic in addition to ensuring that the equations are amenable to asymptotic analysis.

Nondimensional parameter	Default value
k_S, μ	10^{-2}
$\alpha, \lambda, \lambda_a, \eta, \gamma, \gamma_i, \phi, \psi_R, \zeta, u$	1
v, β, β_i	10^2
k_a, ψ_A	10^4
ϵ	10^{-2}

Table 3: The default parameter set. In this work, we concentrate on examining the effects of varying the rate k_i at which inhibitor is introduced to the cells.

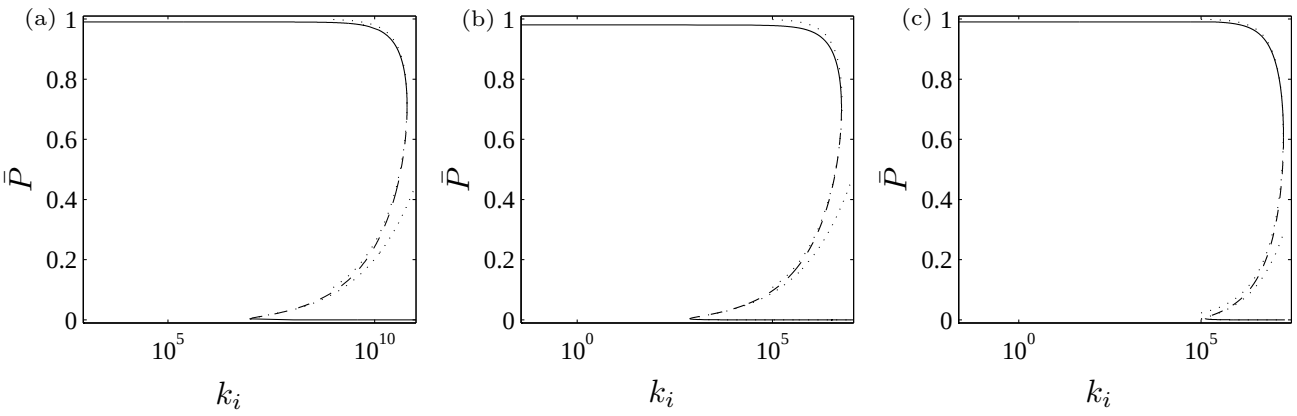

Figure 9: The solid lines (stable) and dashed lines (unstable) represent the steady states of $P(\tau)$, $\bar{P}$, for varying k_i for (a) Model I, (b) Model II and (c) Model III, plotted with the data obtained using XPPAUT 5.91. We plot the data on a log scale in order to be able to see clearly the location of the lower fold bifurcations. The dotted lines are the asymptotic approximations to these solution curves, their derivation being provided in §4 (one captures the upper stable and intermediate unstable steady states, while the other approximates the lower stable steady state). Parameter values are provided in Table 3. While the three cases are qualitatively similar, Model I requires a much larger value of k_i than the other two models to guarantee downregulation and it is thus the least sensitive to suppression by inhibitor. In this respect, Model II has the weakest of the three cascades, as it can (for our parameter set) be suppressed with the lowest value of k_i. We investigate why this might be the case in the context of time-dependent solutions of the three models.

3 Numerical solutions

Our aim is to investigate the effects of inhibitor therapy on the three different cascades of the TCS. We begin by looking at the steady-state profile of P, the proportion of up-regulated cells, as we vary k_i, i.e. the rate, per unit volume and time, at which inhibitor molecules are introduced into the environment of the cells. Figure 9 illustrates the resulting solution curves using our default parameter set; the solid lines represent stable steady states, the dashed lines unstable ones and the dotted lines track the asymptotic approximation to these curves which will be derived in §4.

Each model exhibits three regimes of steady-state behaviour. For lower values of k_i there is not enough inhibitor to block the QS systems and the cells will always reach an up-regulated state (as in [24], where $k_i = 0$). For sufficiently large values of k_i, there is enough inhibitor present to downregulate the cells whatever the initial state. Intermediate values of k_i give bistability, so that the success of inhibitor therapy will be dependent upon the initial conditions of the system, notably on the level of upregulation of the population when the inhibitor is first applied (the position of the unstable branch gives some indication of the basins of attraction): if the operon is in the early stages of self-activation then inhibitor therapy stands a chance of blocking enough receptors to downregulate the operon; however, if the cells have already reached a sufficiently active state at the time that inhibitor molecules are introduced, the receptors will already be predominantly bound to AIP and the inhibitor will be unable to bind to enough receptors to prevent the cells from reaching an active state, albeit one with a slightly reduced level of activity from when no inhibitor is present. This hysteretic behaviour is consistent both with results derived in [25] and with experimental results which illustrate that the crucial step of staphylococcal murine abscess formation is in the initial stages of infection [33]: blocking the *agr* operon with inhibitor molecules during this early phase alone (the half-life of the inhibitor molecules, which are introduced only at the start of the experiment, is short in comparison with the length of time it takes to cause an infection) is sufficient to render the bacteria incapable of forming the abscess as the mice gain increased time to fight the weakened bacteria.

While each of the three cases produces this hysteresis curve, their bistable intervals correspond to considerably different ranges of k_i. Model II has the smallest range and smallest upper and lower limits on the bistable region, followed by Model III and then Model I. Models I and II differ to such an extent that their bistable regions do not overlap. This suggests that the classical TCS cascade, represented by Model I, is more robust to inhibitor therapy than either of the other two, since a much larger value of k_i is required before the inhibitor therapy can have any chance of success. Model II on the other hand, would be most sensitive to the inhibitor and therefore would be the least effective (in the current context) TCS cascade to have evolved in the *agr* operon of the three proposed here. It must be remembered, however, that care is needed when making comparisons between the three models, given that each contains parameters which do not appear in

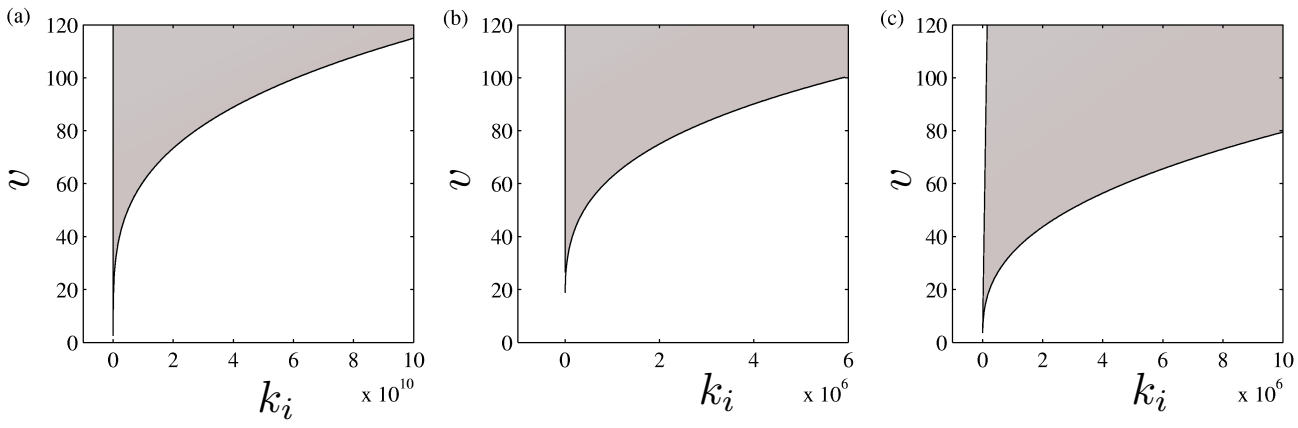

Figure 10: Parameter plots of the fold locations for (a) Model I, (b) Model II and (c) Model III; in each case, the shaded area illustrates the range of k_i that would display bistable behaviour for a given choice of v. The left edge of the shaded area corresponds with the lower fold bifurcation and the right edge with the upper fold bifurcation. For sufficiently small v, the models do not have bistable behaviour and so for a specific value of k_i there will exist only one stable steady state. Our parameter choice ($v = 100$) is consistent with previous mathematical and experimental results which suggest that the *agr* operon is likely to display bistable behaviour.

the others. Nevertheless, if the appropriate data were available such differences would provide some insight into which phosphorylation cascade operates in such TCSs, in particular given the striking difference in the bistable region between Model I and Model II, allowing greater knowledge of when inhibitor therapy may and may not be successful.

We can also track the location of the fold bifurcations as we vary specific parameters (this we do using the package XPPAUT 5.91). For example, Figures 10 and 11 illustrate the fold locations as we vary the parameters v and ψ_A respectively (these parameters are in their unscaled but nondimensional form, as defined in (29)). We choose these parameters to emphasise the mathematical significance of our parameter choice (which in these figures corresponds to $v = 100$ and $\psi_A = 10^4$). We recall that v represents the ratio of the QS-controlled transcription rate to the basal rate, and ψ_A represents the rate of constitutive AgrA phosphorylation (in Model II only). For biological reasons we expect both of these parameters to be large (see §2). In each case, the shaded area represents the parameter regime that displays bistable behaviour. So, for example, for sufficiently small v the fold bifurcations are absent and only a single stable steady state is possible for any given value of k_i. Our parameter choice is therefore consistent with the idea that the *agr* operon would display hysteretic behaviour. Notice that the lower fold in each case varies much less with k_i than does the upper one. The implication of this is that the higher the value of v the larger the bistable region will be, i.e. the minimum value of k_i

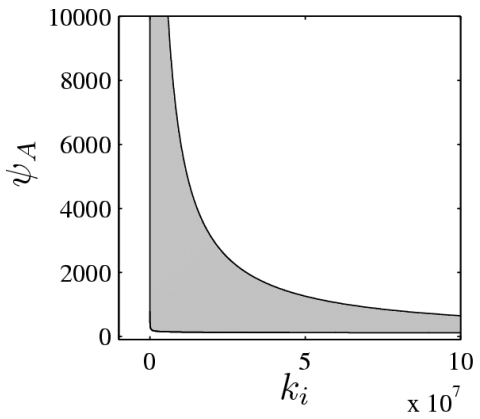

Figure 11: Parameter plot of the fold locations for Model II with varying k_i and ψ_A, the latter parameter representing the rate of constitutive AgrA phosphorylation (we recall that this parameter appears only in Model II). As in Figure 10, the left edge of the shaded area corresponds with the lower fold bifurcation and the right edge with the upper fold bifurcation. Our parameter choice ($\psi_A = 10^4$) is consistent with previous mathematical and experimental results which suggest that the *agr* operon is likely to display bistable behaviour.

at which it is possible for the inhibitor to downregulate the cells does not change markedly (at least relative to the upper fold) while the minimum value of k_i required to *guarantee* downregulation increases greatly with v. Thus increasing the ratio of the rates of QS-controlled transcription to basal transcription is indicative of the cells augmenting their ability to self-activate in spite of the inhibitor. Conversely, *decreasing* ψ_A (see Figure 11) increases this bistable range because more non-phosphorylated AgrA (which is active) will be present in the cells merely because the act of constitutive phosphorylation is slower and not because more has been activated via the phosphorylation cascade. Such comments illustrate how results can be dependent upon parameter choice. For example, taking a sufficiently low value of ψ_A in Model II induces a bistable region comparable with those of Models I and III (although we believe this likely to be biologically inappropriate since activator would be present in the absence of AIP). In spite of the parameter-dependency, this type of comparison enables us to envisage when inhibitor therapy would be successful and how much would be required for each TCS cascade; in §4 we derive analytical expressions for this threshold level.

Figures 12-14 give some time-dependent numerical solutions to each of the three models. To save space only a selection of variables is illustrated. In each case we first demonstrate (Figures 12(a)-14(a)) what happens when no inhibitor is present, using the completely down-regulated steady state (which is described in Appendix A) as the initial condition. The cells quickly reach an up-regulated state, with P approaching 1. The concentrations of all the proteins

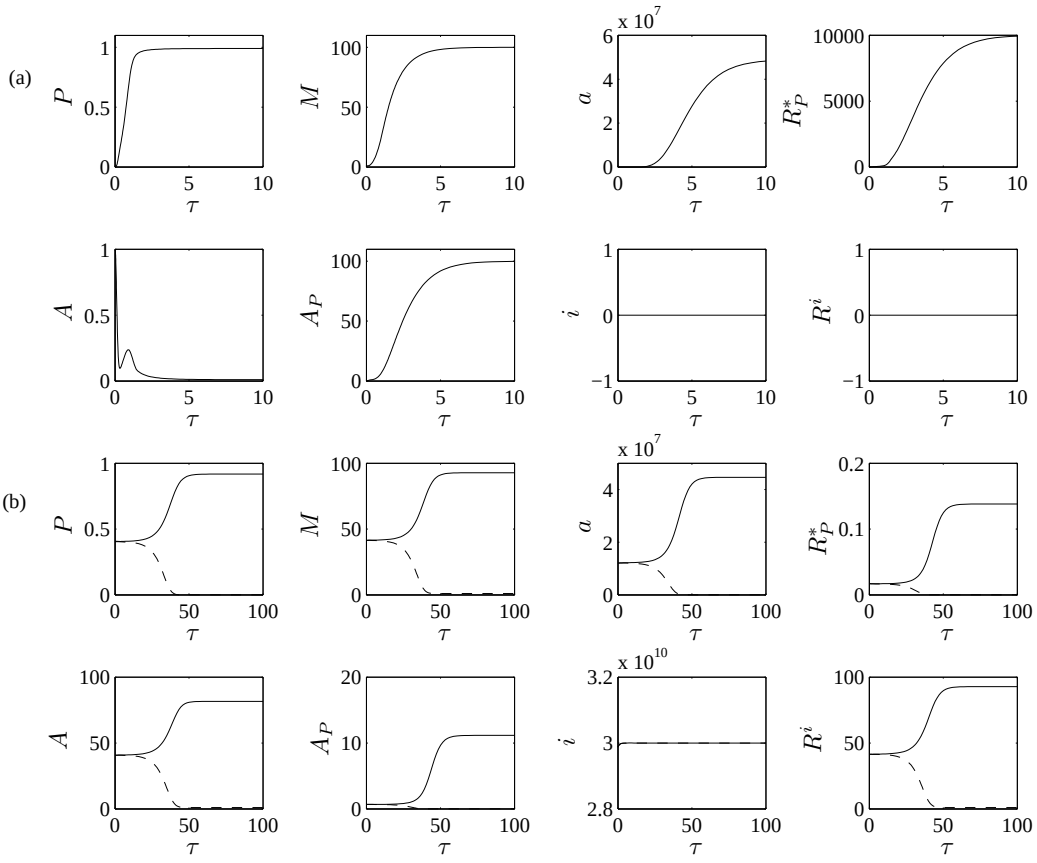

Figure 12: Selected numerical solutions to the nondimensional Model I using the parameters from Table 3. In (a) $k_i = 0$ and (b) $k_i = 3/\epsilon^5$. The initial conditions for (a) are given by (31). For (b), in order to demonstrate the bistable nature of the model, we obtain the initial conditions by perturbing the unstable steady state at $k_i = 3/\epsilon^5$ for each variable either in the direction of its active stable steady state (solid line) or of its inactive stable steady state (dashed line) to obtain the initial conditions.

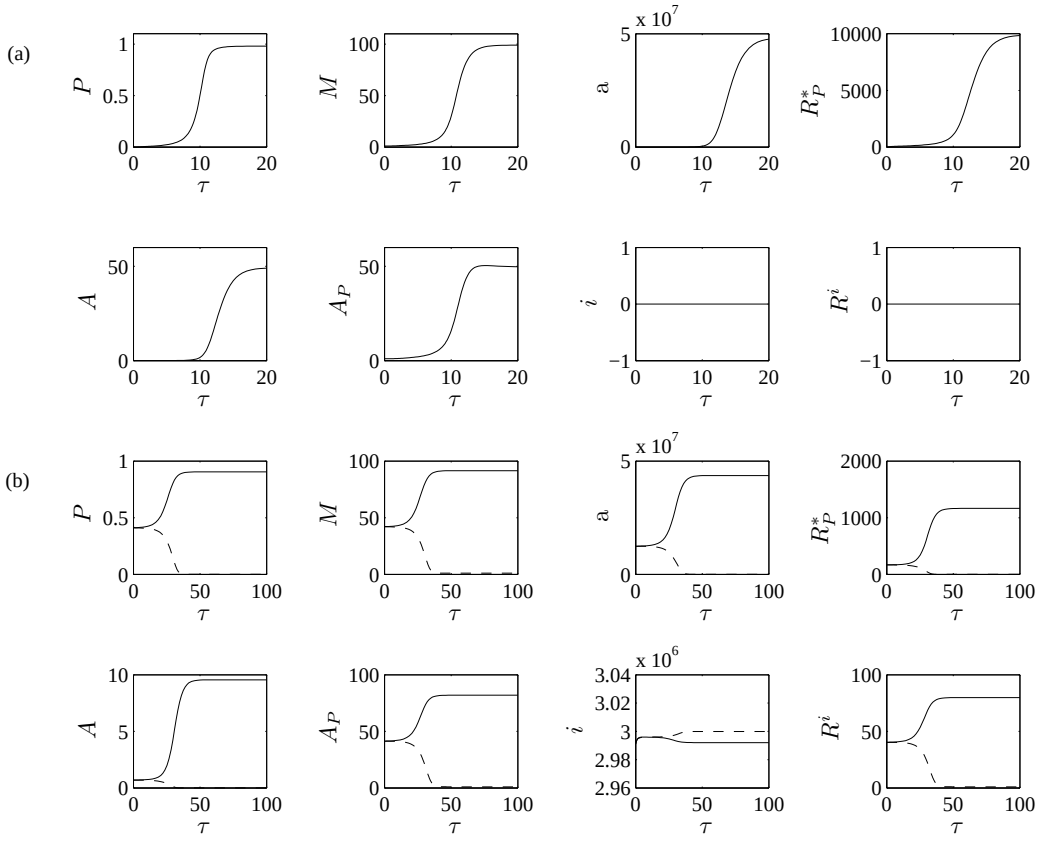

Figure 13: Selected numerical solutions to the nondimensional Model II using the parameters from Table 3. In (a) $k_i = 0$ and (b) $k_i = 3/\epsilon^3$. The initial conditions for (a) are given by (31) and (32), while for (b) we calculate the unstable steady state for $k_i = 3/\epsilon^3$ and for each variable we perturb the state either towards its active stable state (solid line) or its inactive stable state (dashed line) to obtain the initial conditions, thus demonstrating the bistable nature of the model. The inhibitor molecules can downregulate the bacteria of this model at much lower values of k_i. Note that the roles of phosphorylated and non-phosphorylated AgrA are reversed in this model.

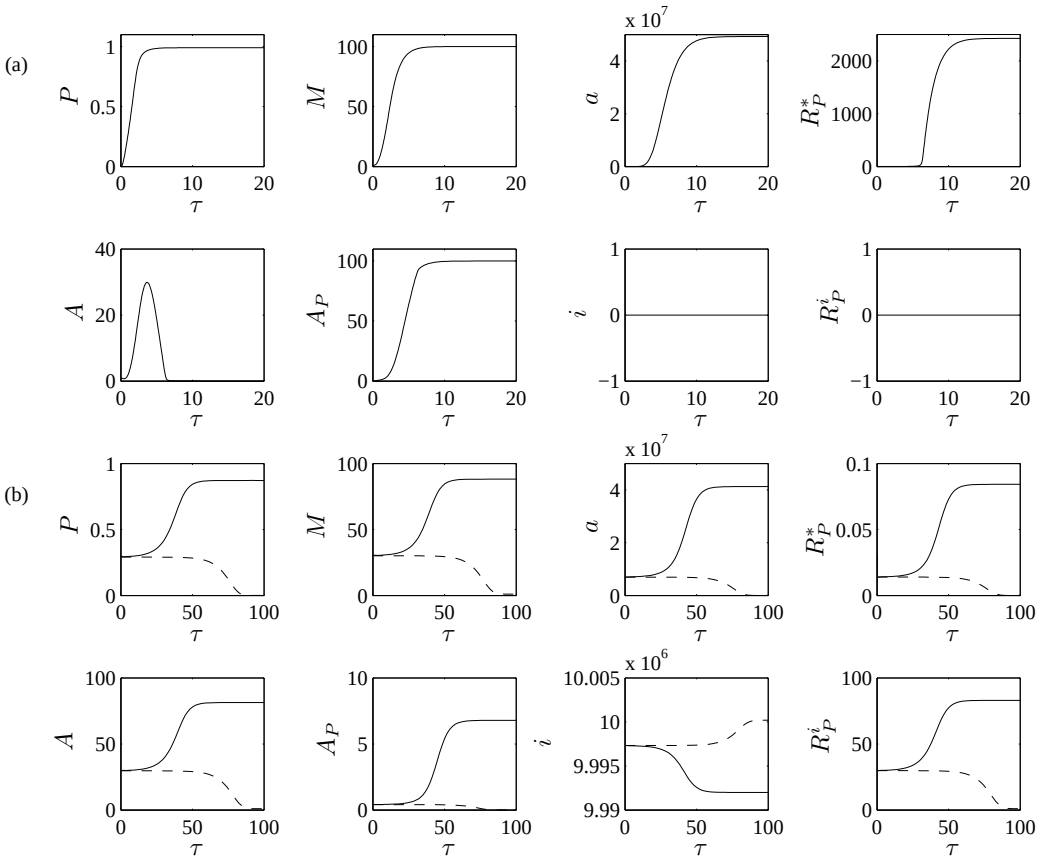

Figure 14: Selected numerical solutions to the nondimensional Model III using the parameters from Table 3. In (a) $k_i = 0$ and (b) $k_i = 10/\epsilon^3$. The initial conditions for (a) are given by (31) and (35), while for (b) we perturb the unstable steady state for $k_i = 10/\epsilon^3$ either towards its active stable state (solid line) or its inactive stable state (dashed line) in order to obtain the initial conditions, thus demonstrating the bistable nature of the model.

except those of inactive AgrA and free receptors (the latter is not shown) increase accordingly. As would be expected, in Models I and III the level of inactive AgrA (i.e., non-phosphorylated AgrA in these cases) decreases to much less than that of active AgrA, and any increase due to synthesis can be seen only early on when the QS loop has yet to take full effect. This increase is much more evident in Model III (see Figure 14(a)). In Model II inactive AgrA is of the phosphorylated form and we see in Figure 13(a) that in this instance the steady state levels of active and inactive AgrA are roughly the same due to the balance between phosphorylation on production and dephosphorylation via activation. We see in Figure 13(b) that once inhibitor is introduced this balance tips in favour of inactive AgrA, since the inhibitor molecules induce lower levels of activation. In each case, the level of unbound receptors decreases dramatically as more and more become bound to AIP molecules. Notice that Model I is the quickest to reach upregulation, followed by Model III and then Model II, i.e. it would seem likely that the sensitivity of the TCS to inhibition is linked to the time the cell takes to become active: the longer this process takes, the more opportunity there is for the inhibitor to suppress the *agr* operon and the larger the bistable region will be.

The second set of solutions in each case (Figures 12(b)-14(b)) demonstrates the bistable behaviour of each model for specific values of k_i. From the data calculated in plotting the bifurcation diagrams, we obtain for each variable the unstable steady state for a given k_i (this value differs in each case since the bistable parameter regime varies with the model) and then perturb the initial condition for each variable either toward the active stable steady state (solid line) or toward the inactive stable steady state (dashed line). It is evident that the cells will either reach a highly active state in which the inhibitor therapy has been unsuccessful, or a suppressed state where inhibitor therapy has clearly taken effect, the former occurring when the initial conditions associated with the *agr* operon are higher. In other words, the lower the activity of the operon when inhibitor therapy is administered, the more potential the therapy has to be effective. For all variables the solutions remain close to the unstable steady state for a time (where the solution appears flat) before diverging towards one of the two stable steady states. We note that it is not possible to distinguish between the active and inactive steady state concentrations of inhibitor, i, in Model I; this result can be manipulated to simplify the model and in §4 we derive the approximation to this steady state which could be used in place of the equation representing the rate of change of inhibitor concentration.

The amount of AIP-bound receptor (R_P^*) that is required to upregulate the cells is a convenient measure of the efficiency of the QS loop: in the presence of inhibitor R_P^* reaches a considerably lower level for all models than in the absence of any inhibitor and for Models I and III there is actually a higher level of inhibitor-bound receptor than its AIP-bound counterpart even when the cell becomes *agr*-active (see the solid lines of Figures 12(b) and 14(b)). Figure 15 illustrates the steady-state curves for R_P^* for each model. Remembering that the entirety of the upper stable section of

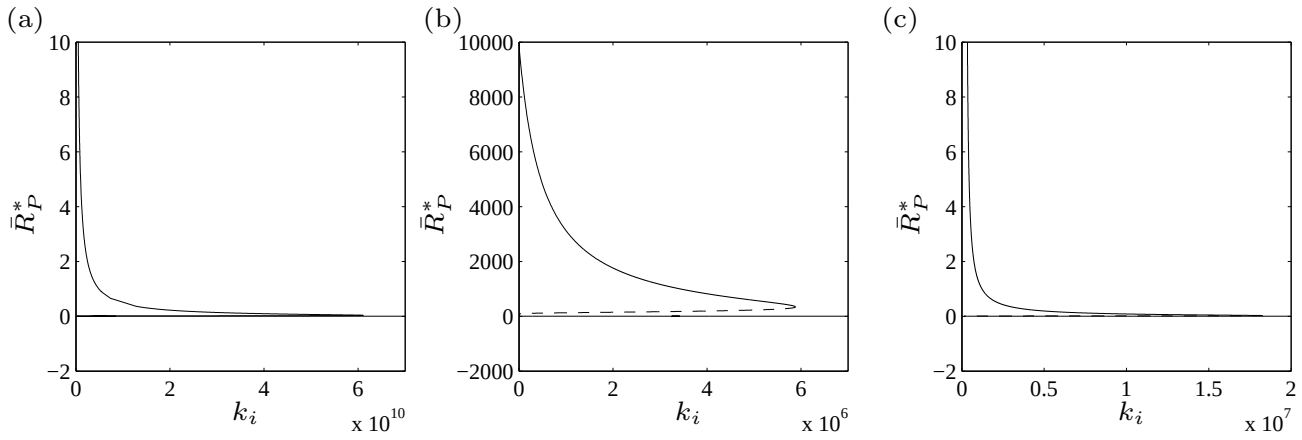

Figure 15: The steady states of $R_P^*(\tau)$, $\bar{R}_P^*$, for varying k_i, solved numerically for (a) Model I, (b) Model II and (c) Model III. Solid lines illustrate stability and dashed ones instability (for Models I and III the unstable branch is not clearly visible due to its proximity to the lower stable curve). Since the highest curve in each case represents an up-regulated population, it is clear that relatively small amounts of AIP-bound receptor are required to upregulate the cell in comparison with the actual level of this complex achieved when no inhibitor is used.

the curve represents an active population, it is clear that the concentration of AIP-bound receptor required to upregulate the cells is not as high as is produced when no inhibitor is present: much smaller quantities will suffice. For Models I and III we have adjusted the y-axis to illustrate clearly the difference between the upper stable branch and the lower two branches. Even so, the drop in the level of $\bar{R}_P^*$ as k_i increases is so drastic for these two models that it is impossible to distinguish between the unstable branch and the lower stable branch in these diagrams.

4 Asymptotic approximation to the steady-state curves

The full steady states of the three models cannot be expressed explicitly; instead, we exploit asymptotic techniques to derive approximations to the steady-state curves of Figure 9 (the approximations are given by the dotted lines) and the corresponding curves for all variables. The approximations are provided in this section, while, for conciseness, their derivations are given only in Appendix B. The scalings of k_i and each variable needed to produce the asymptotic approximation to the active and unstable branches are denoted by $X^\dagger$; when they are scaled to approximate the inactive branch we use $X^\ddagger$. The steady-state approximations for each variable X are denoted $\bar{X}^\dagger$ and $\bar{X}^\ddagger$.

An asymptotic approach enables the inference of more precise information from the models than could be obtained by examining the numerical solutions in isolation. For instance, for each model we obtain analytical estimates of the

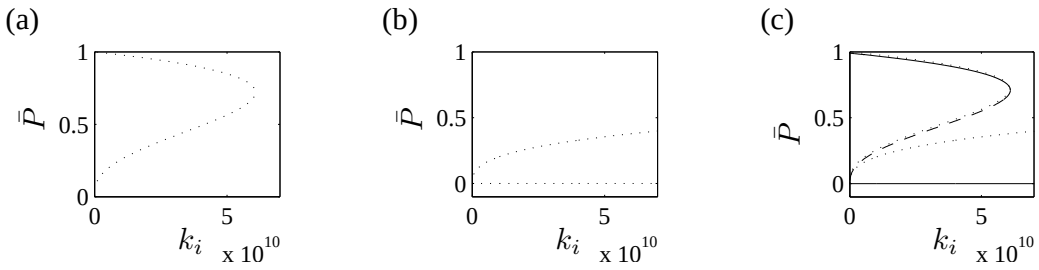

Figure 16: The real and positive roots of equations (a) (9) and (b) (11). These approximate (a) the active stable branch, unstable branch and upper fold bifurcation, and (b) the inactive stable branch and lower fold bifurcation of the solution curve for Model I given in Figure 9(a). In (c) we plot the asymptotic approximations with the full numerical solutions.

threshold levels of inhibitor required for it to be successful in downregulating the *agr* operon (both possible success, initial conditions permitting, and guaranteed success), providing insight into which parameters are predominantly responsible for the efficacy of inhibitor therapy.

4.1 Model I

4.1.1 Active stable branch and unstable branch

The asymptotic approximations to the active stable branch and unstable branch are given by

$$\begin{aligned}
&\bar{M}^\dagger \sim \bar{A}^\dagger \sim \hat{v}\bar{P}^\dagger, \quad \bar{S}^\dagger \sim \frac{\lambda\hat{v}\bar{P}^\dagger}{\lambda+\hat{k}_S\hat{v}\bar{P}^\dagger}, && \bar{a}^\dagger \sim \frac{\hat{k}_a\lambda\hat{v}^2{\bar{P}^\dagger}^2}{(\lambda+\hat{k}_S\hat{v}\bar{P}^\dagger)\lambda_a},\\
&\bar{i}^\dagger \sim \frac{k_i^\dagger}{\lambda_i}, && \bar{R}^\dagger \sim \frac{(\lambda+\gamma_i)\lambda_i\gamma_i\hat{v}\bar{P}^\dagger}{k_i^\dagger}, \quad \bar{R}^{i\dagger} \sim \gamma_i\hat{v}\bar{P}^\dagger,\\
&\bar{A}_P^\dagger \sim \frac{(\lambda+\gamma_i)\lambda_i\gamma_i\hat{v}^4\hat{k}_a{\bar{P}^\dagger}^4}{(\lambda+\gamma)(\lambda+\hat{k}_S\hat{v}\bar{P}^\dagger)\lambda_a k_i^\dagger}, && \bar{R}_P^{*\dagger} \sim \frac{(\lambda+\gamma_i)\lambda\lambda_i\gamma_i\hat{v}^3\hat{k}_a{\bar{P}^\dagger}^3}{(\lambda+\gamma)(\lambda+\hat{k}_S\hat{v}\bar{P}^\dagger)\lambda_a\hat{k}_i},
\end{aligned} \tag{8}$$

where the possible leading-order $\bar{P}^\dagger$ are given by the physically-meaningful roots of

$$(\lambda+\gamma_i)\lambda_i\gamma_i\hat{k}_a\hat{v}^4({\bar{P}^\dagger}^4-{\bar{P}^\dagger}^3)+(\lambda+\gamma)\lambda_a u\hat{k}_S\hat{v}k_i^\dagger\bar{P}^\dagger+(\lambda+\gamma)\lambda\lambda_a u k_i^\dagger=0, \tag{9}$$

(we note that the approximations for $\bar{B},\bar{C},\bar{D}$ and $\bar{T}$ here, and henceforth, are identical to that of $\bar{M}$). It is noteworthy that the gene expression level is fully under the control of the QS loop, basal transcription being negligible (see $\bar{M}^\dagger \sim \hat{v}\bar{P}^\dagger$ in (8)).

Equation (9) has four roots but only two of these are positive and real. One of these approximates the active stable branch and the other the unstable branch. The two roots meet at the fold bifurcation joining these two branches, see Figures 9(a) and 16(a). The location, $(k_{iU}^\dagger, \bar{P}_U^\dagger)$, of this upper bifurcation point is given at leading order by

$$k_{iU}^{\dagger} = \frac{(\lambda+\gamma_i)\lambda_i\gamma_i\hat{k}_a\hat{v}^4(\bar{P}_U^{\dagger 3} - \bar{P}_U^{\dagger 4})}{(\lambda+\gamma)\lambda_a u(\hat{k}_S\hat{v}\bar{P}_U^{\dagger}+\lambda)}, \qquad \bar{P}_U^{\dagger} = \frac{1}{3}\left(1 - \frac{2\lambda}{\hat{k}_S\hat{v}} - \sqrt{\left(1-\frac{2\lambda}{\hat{k}_S\hat{v}}\right)^2 + \frac{9\lambda}{\hat{k}_S\hat{v}}}\right),$$

i.e. the value of k_i at which it can be guaranteed that inhibitor therapy be successful is determined principally (assuming rates of degradation and separation from receptors are comparable between AIP and inhibitor) by the rates of AIP production, mRNA transcription and separation of inhibitor molecules from receptors and of AgrA from the DNA binding site. The only parameter of these which could be optimised, at least to an extent, through the design of the inhibitor molecule is the rate of separation of inhibitor molecules from the receptors, γ_i: minimising this parameter will decrease the value of k_i at which inhibitor success can be guaranteed. Finally, we note that the activation level is determined solely by AIP production, mRNA transcription and degradation rates.

4.1.2 Inactive branch

The asymptotic approximations to the inactive branch are given by

$$\begin{aligned}
&\bar{M}^{\ddagger} \sim \bar{A}^{\ddagger} \sim \bar{S}^{\ddagger} \sim \hat{v}\bar{P}^{\ddagger} + 1, && \bar{a}^{\ddagger} \sim \frac{\hat{k}_a(\hat{v}\bar{P}^{\ddagger}+1)^2}{\lambda_a}, && \bar{i}^{\ddagger} \sim \frac{k_i^{\ddagger}}{\lambda_i},\\
&\bar{R}^{i\ddagger} \sim \gamma_i(\hat{v}\bar{P}^{\ddagger}+1), && \bar{R}^{\ddagger} \sim \frac{(\lambda+\gamma_i)(\hat{v}\bar{P}^{\ddagger}+1)\lambda_i\gamma_i}{k_i^{\ddagger}}, &&\\
&\bar{R}_P^{*\ddagger} \sim \frac{(\lambda+\gamma_i)(\hat{v}\bar{P}^{\ddagger}+1)^3\lambda_i\gamma_i\hat{k}_a}{(\lambda+\gamma)\lambda_a k_i^{\ddagger}}, && \bar{A}_P^{\ddagger} \sim \frac{(\lambda+\gamma_i)(\hat{v}\bar{P}^{\ddagger}+1)^4\lambda_i\gamma_i\hat{k}_a}{(\lambda+\gamma)\lambda\lambda_a k_i^{\ddagger}}, &&
\end{aligned} \tag{10}$$

where $\bar{P}^{\ddagger}$ is given at leading order by a physically-meaningful root of

$$(\lambda+\gamma_i)\lambda_i\gamma_i\hat{k}_a(\hat{v}\bar{P}^{\ddagger}+1)^4 - (\lambda+\gamma)\lambda\lambda_a u k_i^{\ddagger}\bar{P}^{\ddagger} = 0. \tag{11}$$

As with equation (9), (11) has four roots but only two give positive real solutions. This time, the two relevant roots meet at the fold bifurcation joining the inactive branch to the unstable branch, and the lower one of these approximates this inactive branch, see Figures 9(a) and 16(b).

While QS-induced transcription still features at leading order, basal transcription now also appears due to the high proportion of suppressed cells (see $\bar{M}^{\ddagger} \sim \hat{v}\bar{P}^{\ddagger} + 1$ in (10)). Similarly, we do not see the loss of transmembrane AgrD (S) as a result of AIP production in the leading-order behaviour of the inactive cells (the parameter k_S does not feature in our approximation of S in (10)) because when the QS loop is repressed much less AIP is produced. It might seem logical to expect the activating binding reactions (represented by β and η) to be present in the leading-order behaviour of the active cells (i.e. in (8) and (9)) and the inhibitory binding reactions (β_i) to be in that of the repressed cells (in (10) and (11)). However, even in an active state, the activating binding reactions do not come into the leading-order behaviour of these equations. We shall see that this is also the case for Model III, while Model II displays more unexpected behaviour in this respect. The lack of activating binding reactions at leading order in this model demonstrates that the QS circuit

is sufficiently efficient that even when it appears as though the inhibitor molecules are dominating the behaviour, there can still be enough free receptors and AIP molecules to overcome the inhibition, and is consistent with the numerical solutions of Figures 12(b) (and 14(b) for Model III) where final AIP-bound receptor levels are much lower than those of inhibitor-bound receptor even when the cells reach an active state.

The location, $(k_{iL}^{\ddagger}, \bar{P}_L^{\ddagger})$, of the lower fold bifurcation is given at leading order by

$$k_{iL}^{\ddagger} = \frac{256(\lambda+\gamma_i)\lambda_i\gamma_i\hat{k}_a\hat{v}}{27(\lambda+\gamma)\lambda\lambda_a u}, \qquad \bar{P}_L^{\ddagger} = \frac{1}{3\hat{v}},$$

i.e. it is the same parameters governing the threshold value of k_i below which inhibitor therapy is guaranteed to fail as those governing the threshold value of k_i above which it is guaranteed to succeed; here, minimising γ_i will decrease the value of k_i below which inhibitor is guaranteed to fail. In the inactive state, the proportion of active cells is determined (at leading order) simply by the rate of mRNA transcription: since the cell is inactive, the contributions of all other reactions are negligible.

Finally, notice that the approximation for i is the same regardless of whether the operon is active or inactive. We could thus simplify the model by approximating inhibitor concentration by k_i/λ_i (the balance between its production and degradation), in particular if the focus of attention is on the steady states of the system.

4.2 Model II

4.2.1 Active stable branch and unstable branch

The asymptotic approximations to the active stable branch and unstable branch in Model II (where dephosphorylated AgrA is the activator) are

$$\begin{aligned}
&\bar{M}^{\dagger} \sim \hat{v}\bar{P}^{\dagger}, \qquad \bar{S}^{\dagger} \sim \frac{\lambda\hat{v}\bar{P}^{\dagger}}{\lambda+\hat{k}_S\hat{v}\bar{P}^{\dagger}}, \quad \bar{a}^{\dagger} \sim \frac{\hat{k}_a\lambda\hat{v}^2{\bar{P}^{\dagger}}^2}{(\lambda+\hat{k}_S\hat{v}\bar{P}^{\dagger})\lambda_a}, \quad \bar{i}^{\dagger} \sim \frac{k_i^{\dagger}}{\lambda_i},\\
&\bar{R}^{\dagger} \sim \frac{(\lambda+\gamma_i)\lambda_i\gamma_i\hat{v}\bar{P}^{\dagger}}{k_i^{\dagger}}, \quad \bar{R}_P^{*\dagger} \sim \frac{(\lambda+\gamma_i)\lambda\lambda_i\gamma_i\hat{v}^3\hat{k}_a{\bar{P}^{\dagger}}^3}{(\lambda+\gamma)(\lambda+\hat{k}_S\hat{v}\bar{P}^{\dagger})\lambda_a k_i^{\dagger}}, \quad \bar{R}^{i\dagger} \sim \gamma_i\hat{v}\bar{P}^{\dagger},\\
&\bar{A}^{\dagger} \sim \frac{(\lambda+\gamma_i)\lambda\lambda_i\gamma_i\phi\hat{k}_a\hat{v}^4{\bar{P}^{\dagger}}^4}{(\lambda+\gamma)(\lambda+\hat{k}_S\hat{v}\bar{P}^{\dagger})\lambda_a\hat{\psi}_A k_i^{\dagger}}, \quad \bar{A}_P^{\dagger} \sim \frac{\hat{v}\bar{P}^{\dagger}}{\phi},
\end{aligned} \tag{12}$$

where the possible leading-order $\bar{P}^{\dagger}$ are given by the physically-meaningful roots of

$$(\lambda+\gamma_i)\lambda\lambda_i\gamma_i\hat{k}_a\hat{v}^4({\bar{P}^{\dagger}}^4 - {\bar{P}^{\dagger}}^3) + (\lambda+\gamma)\lambda_a u\hat{\psi}_A\hat{k}_S\hat{v}\hat{k}_i\bar{P}^{\dagger} + (\lambda+\gamma)\lambda\lambda_a u\hat{\psi}_A k_i^{\dagger} = 0. \tag{13}$$

Only the approximations for $\bar{A}^{\dagger}$, $\bar{A}_P^{\dagger}$ and $\bar{P}^{\dagger}$ differ from Model I: here AgrA levels are governed by constitutive phosphorylation and activation, rather than translation and degradation as in Model I. The two positive real roots of (13) represent the upper stable branch and the unstable branch of the solution curve, meeting at the fold bifurcation which joins these

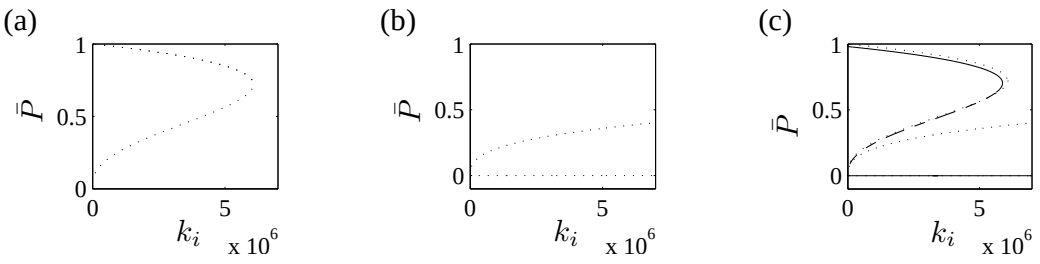

Figure 17: The positive real roots of equations (a) (13) and (b) (16). These approximate (a) the active stable branch, unstable branch and upper fold bifurcation, and (b) the inactive stable branch and lower fold bifurcation of the solution curve for Model II given in Figure 9(b). In (c) we plot the asymptotic approximations with the full numerical solutions.

two branches, see Figures 9(b) and 17(a), which, at leading order, occurs at

$$k_{iU}^{\dagger} = \frac{(\lambda+\gamma_i)\lambda\lambda_i\gamma_i\hat{k}_a\hat{v}^4(\bar{P}_U^{\dagger 3} - \bar{P}_U^{\dagger 4})}{(\lambda+\gamma)\lambda_a u\hat{\psi}_A(\hat{v}\hat{k}_S\bar{P}_U^{\dagger}+\lambda)}, \qquad \bar{P}_U^{\dagger} = \frac{1}{3}\left(1 - \frac{2\lambda}{\hat{v}\hat{k}_S} - \sqrt{\left(1-\frac{2\lambda}{\hat{v}\hat{k}_S}\right)^2 + \frac{9\lambda}{\hat{v}\hat{k}_S}}\right);$$

this, again, is very similar to Model I: the parameter groupings are the same with the exception of a dependence upon $\hat{\psi}_A$, the rate of constitutive phosphorylation of AgrA, in Model II. The level of inhibitor required to ensure downregulation of the *agr* operon (regardless of initial conditions) decreases with increasing $\hat{\psi}_A$. It would, therefore, be tempting to speculate that a Model II TCS would be stronger if $\hat{\psi}_A$ were smaller, but the result of this would be that increased levels of active AgrA would be present constitutively and not as a consequence of an active *agr* operon, thus defeating the purpose of the signal transduction system.

4.2.2 Inactive branch

The asymptotic approximations for the inactive stable branch of Model II are

$$\begin{aligned}
&\bar{M}^{\ddagger} \sim \bar{S}^{\ddagger} \sim \hat{v}\bar{P}^{\ddagger}+1, \quad \bar{A}^{\ddagger} \sim \frac{\phi\hat{k}_a(\hat{v}\bar{P}^{\ddagger}+1)^3\bar{R}^{\ddagger}}{\hat{\psi}_A(\hat{\beta}\lambda\bar{R}^{\ddagger}+(\lambda+\gamma)\lambda_a)}, \quad \bar{a}^{\ddagger} \sim \frac{(\lambda+\gamma)\hat{k}_a(\hat{v}\bar{P}^{\ddagger}+1)^2}{(\hat{\beta}\lambda\bar{R}^{\ddagger}+(\lambda+\gamma)\lambda_a)},\\
&\bar{A}_P^{\ddagger} \sim \frac{1}{\phi}(\hat{v}\bar{P}^{\ddagger}+1), \qquad \bar{R}_P^{*\ddagger} \sim \frac{\hat{k}_a(\hat{v}\bar{P}^{\ddagger}+1)^2\bar{R}^{\ddagger}}{(\hat{\beta}\lambda\bar{R}^{\ddagger}+(\lambda+\gamma)\lambda_a)}, \qquad \bar{i}^{\ddagger} \sim \frac{(\lambda+\gamma_i)k_i^{\ddagger}}{(\hat{\beta}_i\lambda\bar{R}^{\ddagger}+(\lambda+\gamma_i)\lambda_i)},\\
&\bar{R^i}^{\ddagger} \sim \frac{k_i^{\ddagger}\bar{R}^{\ddagger}}{(\hat{\beta}_i\lambda\bar{R}^{\ddagger}+(\lambda+\gamma_i)\lambda_i)},
\end{aligned} \tag{14}$$

where $\bar{P}^{\ddagger}$ and $\bar{R}^{\ddagger}$ are given at leading order by

$$\begin{aligned}
&\lambda\bar{R}^{\ddagger 2}\left[\hat{\beta}^2\hat{\beta}_i\lambda\gamma_i(\hat{v}\bar{P}^{\ddagger}+1) - \hat{\beta}_i\gamma_i\hat{\eta}\hat{k}_a(\hat{v}\bar{P}^{\ddagger}+1)^2 - \hat{\beta}^2k_i^{\ddagger}\right]\\
&+\bar{R}^{\ddagger}\left[(\hat{v}\bar{P}^{\ddagger}+1)((\lambda+\gamma_i)\hat{\beta}^2\lambda\lambda_i\gamma_i + (\lambda+\gamma)\hat{\beta}\hat{\beta}_i\lambda\lambda_a\gamma_i) - (\lambda+\gamma_i)\lambda_i\gamma_i\hat{\eta}\hat{k}_a(\hat{v}\bar{P}^{\ddagger}+1)^2 - (\lambda+\gamma)\hat{\beta}\lambda_a k_i^{\ddagger}\right]\\
&+(\lambda+\gamma)(\lambda+\gamma_i)\hat{\beta}\lambda_a\lambda_i\gamma_i(\hat{v}\bar{P}^{\ddagger}+1) = 0,
\end{aligned} \tag{15}$$

$$\bar{P}^{\ddagger} = \frac{\hat{k}_a(\hat{v}\bar{P}^{\ddagger}+1)^3\bar{R}^{\ddagger}}{\hat{\psi}_A u(\hat{\beta}\lambda\bar{R}^{\ddagger}+(\lambda+\gamma)\lambda_a)}; \tag{16}$$

eliminating $\bar{R}^\ddagger$ gives a 7th order polynomial in $\bar{P}^\ddagger$. Solving (15) and (16) produces only two meaningful roots, which join at the lower fold bifurcation; one of these provides an approximation to the inactive stable branch, see Figures 9(b) and 17(b). It is possible to derive an expression for the location of the lower fold bifurcation as the solution to a 5th order polynomial, omitted for brevity.

As mentioned in §4.1, we now see some unexpected results in terms of the leading-order binding reactions. In the active state, only the inhibitory binding reactions played a part in the dominant behaviour of the system (see the dependence on γ_i in (12) and (13). However, in the suppressed state, the activating binding reactions also appear at leading order (β, β_i, γ and γ_i all play a role in (14)-(16)), whereas one might anticipate that, if they were going to arise, we would see the activating binding reactions in the active state (i.e. in (12) and (13)). This can be understood if we bear in mind that the active and inactive systems capture the behaviour of the cells in the region of the fold bifurcations. The upper fold bifurcation (on the active branch) represents the threshold level of inhibitor above which the inhibitor will certainly suppress the *agr* operon. The lower fold bifurcation (on the inactive branch) represents the threshold level of inhibitor below which the *agr* operon cannot be suppressed, i.e. where AIP dominates over inhibitor. Though non-intuitive at first, it is actually therefore reasonable that the activating binding reactions should appear at leading order on the lower branch, alongside the inhibitory ones. This behaviour is not seen in Models I or III because inhibitor levels are much larger in comparison to Model II, preventing the AIP-binding reactions from being dominant at leading order.

4.3 Model III

4.3.1 Active stable branch and unstable branch

We recall that this model requires additional variables to model the various phosphorylation states in which transmembrane AgrC can lie. Despite the extra variables, the leading-order reactions are very similar to Model I. Of those which are directly comparable, the only noteworthy difference is the appearance at leading-order of the loss of AIP-bound receptor through activation (in this model) rather than degradation (as happens in Model I). This difference makes the asymptotic approximations for certain variables in Model III appear quite different to the previous two models:

$$\begin{aligned}
&\bar{M}^\dagger \sim \bar{A}^\dagger \sim \bar{R}^\dagger \sim \hat{v}\bar{P}^\dagger, \quad \bar{S}^\dagger \sim \frac{\lambda\hat{v}\bar{P}^\dagger}{\lambda+\hat{k}_S\hat{v}\bar{P}^\dagger}, \qquad \bar{a}^\dagger \sim \frac{\hat{k}_a\lambda\hat{v}^2{\bar{P}^\dagger}^2}{(\lambda+\hat{k}_S\hat{v}\bar{P}^\dagger)\lambda_a},\\
&\bar{i}^\dagger \sim \frac{k_i^\dagger}{\lambda_i}, \quad \bar{R}_P^{i\dagger} \sim \gamma_i\hat{v}\bar{P}^\dagger, \quad \bar{R}_P^\dagger \sim \frac{\lambda_i\gamma_i\hat{v}(\lambda+\gamma_i)\bar{P}^\dagger}{k_i^\dagger}, \quad \bar{R}_P^{*\dagger} \sim \frac{(\lambda+\gamma_i)\eta\zeta\lambda\lambda_i\hat{v}^2\hat{k}_a{\bar{P}^\dagger}^2}{\hat{\beta}\lambda_a(\lambda+\hat{k}_S\hat{v}\bar{P}^\dagger)},\\
&\bar{R}^{*\dagger} \sim \frac{\eta\zeta\lambda\lambda_i(\lambda+\gamma_i)\hat{k}_a\hat{v}^3{\bar{P}^\dagger}^3}{\hat{\beta}\lambda_a(\lambda+\hat{k}_S\hat{v}\bar{P}^\dagger)(\lambda+\gamma)}, \qquad \bar{A}_P^\dagger \sim \frac{\eta\zeta\lambda_i\gamma_i(\lambda+\gamma_i)\hat{k}_a\hat{v}^3{\bar{P}^\dagger}^3}{\hat{\beta}k_i^\dagger\lambda_a(\lambda+\hat{k}_S\hat{v}\bar{P}^\dagger)},
\end{aligned} \tag{17}$$

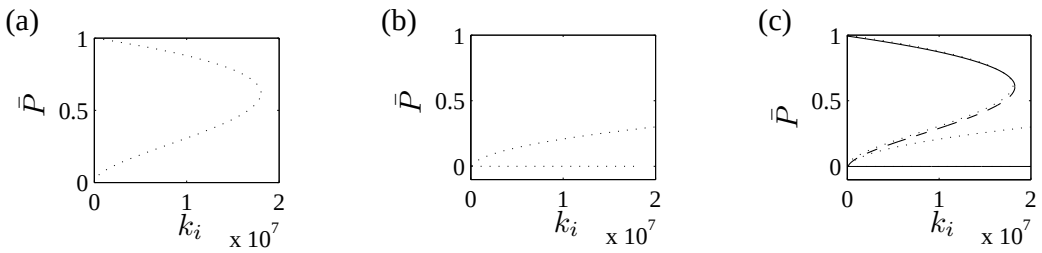

Figure 18: The roots of equations (a) (18) and (b) (20) which are both positive and real, i.e. the physically meaningful roots. These approximate (a) the active stable branch, unstable branch and upper fold bifurcation, and (b) the inactive stable branch and lower fold bifurcation of the solution curve for Model III given in Figure 9(c). In (c) we plot the asymptotic approximations with the full numerical solutions.

where at leading order $\bar{P}^\dagger$ is given by the roots of the cubic

$$(\lambda+\gamma_i)\eta\zeta\lambda_i\gamma_i\hat{k}_a\hat{v}^3({\bar{P}^\dagger}^3-\bar{P}^{\dagger 2})+\lambda_a u\hat{\beta}k_i^\dagger(\lambda+\hat{k}_S\hat{v}\bar{P}^\dagger)=0 \tag{18}$$

which has two real positive solutions approximating the active branch and the unstable branch: see Figures 9(c) and 18(a). The upper fold bifurcation occurs at leading order at

$$k_{iU}^\dagger=\frac{(\lambda+\gamma_i)\lambda_i\gamma_i\eta\zeta\hat{k}_a\hat{v}^3(\bar{P}_U^{\dagger 2}-\bar{P}_U^{\dagger 3})}{\lambda_a u\hat{\beta}(\hat{k}_S\hat{v}\bar{P}_U^\dagger+\lambda)},\qquad \bar{P}_U^\dagger=\frac{1}{4}\left(1-\frac{3\lambda}{\hat{k}_S\hat{v}}+\sqrt{\left(1-\frac{3\lambda}{\hat{k}_S\hat{v}}\right)^2+\frac{16\lambda}{\hat{k}_S\hat{v}}}\right).$$

Thus the key parameters determining the threshold level of inhibitor above which inhibitor therapy will always suppress the *agr* operon are similar to those of Model I but, in addition, the combination of parameters representing the rate of AgrA activation ($\hat{\beta}/\eta\zeta$) in Model III will also affect this threshold level; the same applies to the approximation to the lower fold bifurcation, (21), given below in §5.

4.3.2 Inactive branch

The following asymptotic expressions approximate the inactive branch for Model III:

$$\begin{aligned}
&\bar{M}^\ddagger\sim\bar{A}^\ddagger\sim\bar{R}\sim\bar{S}\sim\hat{v}\bar{P}^\ddagger+1, && \bar{a}^\ddagger\sim\frac{\hat{k}_a(\hat{v}\bar{P}^\ddagger+1)^2}{\lambda_a}, && \bar{i}^\ddagger\sim\frac{k_i^\ddagger}{\lambda_i},\\
&\bar{R}_P^\ddagger\sim\frac{\lambda_i\gamma_i(\lambda+\gamma_i)(\hat{v}\bar{P}^\ddagger+1)}{k_i^\ddagger}, && \bar{R}_P^{i\ddagger}\sim\frac{\lambda_i\gamma_i(\lambda+\gamma_i)(\hat{v}\bar{P}^\ddagger+1)}{k_i^\ddagger},\\
&\bar{R}_P^{*\ddagger}\sim\frac{\eta\zeta\lambda_i\gamma_i\hat{k}_a(\lambda+\gamma_i)(\hat{v}\bar{P}^\ddagger+1)^2}{\hat{\beta}\lambda_a k_i^\ddagger}, && \bar{R}^{*\ddagger}\sim\frac{\eta\zeta\lambda_i\gamma_i\hat{k}_a(\lambda+\gamma_i)(\hat{v}\bar{P}^\ddagger+1)^3}{\hat{\beta}\lambda_a k_i^\ddagger(\lambda+\gamma)},\\
&\bar{A}_P^\ddagger\sim\frac{\eta\zeta\lambda_i\gamma_i\hat{k}_a(\lambda+\gamma_i)(\hat{v}\bar{P}^\ddagger+1)^3}{\hat{\beta}\lambda\lambda_a k_i^\ddagger}, &&
\end{aligned} \tag{19}$$

where at leading order $\bar{P}^\ddagger$ is given by the roots of the cubic

$$(\lambda+\gamma_i)\eta\zeta\lambda_i\gamma_i\hat{k}_a(\hat{v}\bar{P}^\ddagger+1)^3-\lambda\lambda_a u\hat{\beta}k_i^\ddagger\bar{P}^\ddagger=0, \tag{20}$$

which has two positive real solutions. These two roots meet at the lower fold bifurcation and one follows the unstable branch, see Figures 9(c) and 18(b). This lower fold bifurcation at leading order occurs at

$$k_{iL}^{\ddagger} = \frac{27(\lambda+\gamma_i)\eta\zeta\lambda_i\gamma_i\hat{k}_a\hat{v}}{4\lambda\lambda_a u\hat{\beta}}, \qquad P_L^{\ddagger} = \frac{1}{2\hat{v}}. \tag{21}$$

The differences between the active and inactive leading-order reactions for Model III are equivalent to those discussed for Model I, namely the absence of basal transcription in the active cells and the loss of transmembrane AgrD through AIP production in the inactive cells. Additionally, as for Model I, the inhibitor concentration has the same asymptotic approximation for both the stable branches, thus providing a means by which to simplify the model.

We have been able to derive analytical expressions for the steady states of each of the models both when the *agr* operon reaches an active state and when inhibitor therapy is successful in forcing the operon into an inactive state. These expressions can be used for further study of the operon and, since the analysis reveals which parameters govern the threshold levels of inhibitor therapy, in the design of synthetic inhibitor molecules.

5 Discussion

We have examined the impact of a novel approach for combatting bacterial infection by developing models of three potential TCS cascades of the *agr* operon (the primary operon involved in the regulation of virulence factors in *S. aureus* and prevalent in many other pathogens), demonstrating the ease of testing biological hypotheses with mathematical models. In each case we saw bistable behaviour by the cells in response to the inhibitor therapy, making its success dependent on not only the rate, k_i, at which inhibitor was introduced into the bacteria, but also the initial conditions of the system. The implication of this is that, unless k_i can be increased sufficiently, this type of staphylococcal QS inhibition may only be useful as a therapy if it can be implemented in the early stages of infection, otherwise the autoinductive nature of the QS circuit is so efficient that the *agr* operon and thus the population of bacteria will still reach (or remain in) an active and virulent state regardless of inhibitor molecule concentration. This would clearly be a major drawback if QS inhibition were to be used as a therapy against bacterial infections and this complements the experimental results of [33] which demonstrate the importance of suppressing the *agr* operon in the initial stages of infection to prevent staphylococcal abscess formation in a mouse. Although downregulation could be guaranteed for large enough values of k_i (so that the models lose their bistability), it is important to bear in mind that (aside from cost-effectiveness) there would presumably be a maximum amount of these inhibitor molecules that could be introduced to an infection site before they have adverse consequences upon the host.

Using numerical solutions we have shown that the dosage required for inhibitor therapy to be successful is heavily

dependent upon the phosphorylation cascade of the TCS and have identified which of the three cascades is likely to be the most susceptible to inhibitor therapy and which is likely to be the most robust: the classical cascade, of the three, is the best equipped to evade inhibitor therapy and the Model II cascade (where AgrA is constitutively phosphorylated) is the weakest in this respect. It is clear that the Model II cascade is the least efficient of the three, since AgrA must be converted from its active form to an inactive state and then back to its active form, whereas AgrA in the other models simply goes from inactive to active. This would explain why Model II takes the longest to reach an active state, thus rendering it the most susceptible to inhibition. The Model III cascade also requires additional steps but these concern the transition between different phosphorylation states of the receptor, as opposed to the activator, hence making it more vulnerable to inhibition than Model I because its phosphorylation cascade is less efficient, but stronger than Model II because its inefficiency only indirectly affects activator levels (whereas that of Model II lies in the actual activator dynamics).

Given the large differences between the models, if the appropriate (even only semi-quantitative) experimental data were available, these investigations into the effect of inhibitor therapy on the different types of TCS cascade would provide an insight into which cascade is in operation in a particular strain of *S. aureus* or alternative species. Furthermore, if the TCS cascade mechanism of the strain of interest is already known, numerical investigations should help estimate the amount of inhibitor therapy required to suppress an infection successfully. Additionally, our asymptotic analysis in §4 indicates which parameters are primarily responsible for determining the efficacy of inhibitor therapy. Of these, only the rate of separation of inhibitor and receptor could be influenced through the design of the inhibitor. Interestingly, however, the rate of binding between inhibitor and receptor affects the leading-order behaviour of the cells at steady state only in one scenario (Model II when the cells were suppressed); according to our analysis, targetting the rate of separation should be much more effective in enhancing the potency of inhibitor therapy.

It is becoming increasingly clear that *agr*-like QS systems are employed by many Gram-positive bacteria, including a number of important pathogens. Although the focus of this study has been on *S. aureus*, the discovery of *agr* systems in the clostridial species has comparable significance: *C. difficile* has, in recent years, parallelled *S. aureus* in terms of nosocomial infections. Although the contribution of *agr* to virulence gene regulation in *C. difficile* and hence infection are not yet known, *agr* systems regulate virulence factors in enterococci [34], *Listeria* [8] and *C. perfringens* [6]. Hence the importance of understanding the *agr* operon extends far beyond its significance in *S. aureus* alone, not only for its medical implications but for fundamental questions of intra- and inter-species bacterial signalling. Similarly, TCSs are prevalent throughout the bacterial kingdom, and while we have chosen to study TCSs in the context of the *agr* operon, the results (for instance in comparing the robustness of the three TCS cascades) are likely to be transferable across different systems.

Acknowledgements

The authors wish to thank Adrian J. Koerber for all his helpful discussions. S.J. gratefully acknowledges support from BBSRC for this work in the form of a studentship and for subsequent funding under the SysMO initiative. All time-dependent numerical solutions were computed using the ode15s solver in MATLAB v. 7.1 (The MathWorks, Inc.) and bifurcation diagrams were generated using XPPAUT 5.91.

References

[1] Wilson M., McNab R., Henderson B., Bacterial disease mechanisms, an introduction to cellular microbiology, Cambridge University Press, 2002.

[2] Stock A.M., Robinson V.L., Goudreau P.N., Two-component signal transduction, Annu. Rev. Biochem. 69 (2000) 183–215.

[3] Ji G., Beavis R.C., Novick R.P., Cell density control of staphylococcal virulence mediated by an octapeptide pheromone, Proc. Natl. Acad. Sci. USA 92 (1995) 12055–12059.

[4] Salmond G.P.C., Bycroft B.W., Stewart G.S.A.B., Williams P., The bacterial 'enigma': cracking the code of cell-cell communication, Mol. Microbiol. 16 (1995) 615–624.

[5] Sebaihia M., Peck M.W., Minton N.P. *et al.*, Genome sequence of a proteolytic (Group I) *Clostridium botulinum* strain Hall A and comparative analysis of the clostridial genomes, Genome Res. 17 (2007) 1082–1092.

[6] Ohtani K., Yuan Y., Hassan S., Wang R., Wang Y., Shimizu T., Virulence gene regulation by the *agr* system in *Clostridium perfringens*, J. Bacteriol. 191 (2009) 3919–3927.

[7] Podbielski A., Kreikemeyer B., Cell density-dependent regulation: basic principles and effects on the virulence of Gram-positive cocci, Int. J. Infect. Dis. 8 (2004) 81–95.

[8] Riedel C.U., Monk I.R., Casey P.G., Waidmann M.S., Gahan C.G.M., Hill C., AgrD-dependent quorum sensing affects biofilm formation, invasion, virulence and global gene expression profiles in *Listeria monocytogenes*, Mol. Microbiol. 71 (2009) 1177–1189.

[9] Novick R.P., Autoinduction and signal transduction in the regulation of staphylococcal virulence, Mol. Microbiol. 48 (2003) 1429–1449.

[10] Novick R.P., Geisinger E., Quorum sensing in Staphylococci, Annu. Rev. Genet. 42 (2008) 541–64.

[11] Zhang L., Gray L., Novick R.P., Ji G., Transmembrane topology of AgrB, the protein involved in the post-translational modification of AgrD in *Staphylococcus aureus*, J. Biol. Chem. 277 (2002) 34736–34742.

[12] Lina G., Jarraud S., Ji G., Greenland T., Pedraza A., Etienne J., Novick R.P., Vandenesch F., Transmembrane topology and histidine protein kinase activity of AgrC, the *agr* signal receptor in *Staphylococcus aureus*, Mol. Microbiol. 28 (1998) 655–662.

[13] Recsei P., Kreiswirth B., O'Reilly M., Schlievert P., Gruss A., Novick R.P., Regulation of exoprotein gene expression in *Staphylococcus aureus* by *agr*, Mol. Gen. Genet. 202 (1986) 58–61.

[14] Novick R.P., Ross H.F., Projan S.J., Kornblum J., Kreiswirth B., Moghazeh S., Synthesis of staphylococcal virulence factors is controlled by a regulatory RNA molecule, EMBO J. 12 (1993) 3967–3975.

[15] Van Wamel W.J.B., van Rossum G., Verhoef J., Vandenbroucke-Grauls C.M.J.E., Fluit A.C., Cloning and characterization of an accesory gene regulator (*agr*)-like locus from *Staphylococcus epidermidis*, FEMS Microbiol. Lett. 163 (1998) 1–9.

[16] Otto M., Echner H., Voelter W., Götz F., Pheromone cross-inhibition between *Staphylococcus aureus* and *Staphylococcus epidermidis*, Infect. Immun. 69 (2001) 1957–1960.

[17] McDowell P., Affas Z., Reynolds C., Holden M.T.G., Wood S.J., Saint S., Cockayne A., Hill P.J., Dodd C.E.R., Bycroft B.W., Chan W.C., Williams P., Structure, activity and evolution of the group I thiolactone peptide quorum-sensing system of *Staphylococcus aureus*, Mol. Microbiol. 41 (2001) 503–512.

[18] Martin C.A., Hoven A.D., Cook A.M., Therapeutic frontiers: preventing and treating infectious diseases by inhibiting bacterial quorum sensing, Eur. J. Clin. Microbiol. Infect. Dis. 27 (2008) 635–642.

[19] Uroz S., Dessaux Y., Oger P., Quorum sensing and quorum quenching: the yin and yang of bacterial communication, ChemBioChem 10 (2009) 205–216.

[20] Mayville P., Ji G., Beavis R., Yang H., Goger M., Novick R.P., Muir T.W., Structure-activity analysis of synthetic autoinducing thiolactone peptides from *Staphylococcus aureus* responsible for virulence, Proc. Natl. Acad. Sci. USA 96 (1999) 1218–1223.

[21] George E.A., Muir T.W., Molecular mechanisms of *agr* quorum sensing in virulent staphylococci, ChemBioChem. 8 (2007) 847–855.

[22] Cisar E.A.G., Geisinger E., Muir T.W., Novick R.P., Symmetric signalling within asymmetric dimers of the *Staphylococcus aureus* receptor histidine kinase AgrC, Mol. Microbiol. 74 (2009) 44–57.

[23] Koenig R.L., Ray J.L., Maleki S.J., Smeltzer M.S., Hurlburt B.K., *Staphylococcus aureus* AgrA binding to the RNAIII-*agr* regulatory region, J. Bacteriol. 186 (2004) 7549–7555.

[24] Jabbari S., King J.R., Williams P., Mathematical modelling of the *agr* operon in *Staphylococcus aureus*, J. Math. Biol.DOI:10.1007/s00285-009-0291-6.

[25] Gustafsson E., Nilsson P., Karlsson S., Arvidson S., Characterizing the dynamics of the quorum-sensing system in *Staphylococcus aureus*, J. Mol. Microbiol. Biotechnol. 8 (2004) 232–242.

[26] Jabbari S., Mathematical modelling of quorum sensing and its inhibition in *Staphylococcus aureus*, Ph.D. thesis, University of Nottingham, UK (2007).

[27] Lyon G.J., Wright J.S.,Christopoulos A., Novick R.P., Muir T.W., Reversible and specific extracellular antagonism of receptor-histidine kinase signaling, J. Biol. Chem. 277 (2002) 6247–6253.

[28] Alon U., An introduction to systems biology: Design principles of biological circuits, Chapman and Hall/CRC, 2006.

[29] Anguige K., King J.R., Ward J.P., Modelling antibiotic- and anti-quorum sensing treatment of a spatially-structured *Pseudomonas aeruginosa* population, J. Math. Biol. 51 (2005) 557–594.

[30] Dockery J.D., Keener J.P., A mathematical model for quorum sensing in *Pseudomonas Aeruginosa*, Bull. Math. Biol. 63 (2001) 95–116.

[31] Fagerlind M.G., Rice S.A., Nilsson P., Harlén M., James S., Charlton T., Kjelleberg S., The role of regulators in the expression of quorum-sensing signals in *Pseudomonas aeruginosa*, J. Mol. Microbiol. Biotechnol. 6 (2003) 88–100.

[32] James S., Nilsson P., James G., Kjelleberg S., Fagerström T., Luminescence control in the marine bacterium *Vibrio fischeri*: an analysis of the dynamics of *lux* regulation, J. Mol. Biol. 296 (2000) 1127–1137.

[33] Wright III J.S., Jin R., Novick R.P., Transient interference with staphylococcal quorum sensing blocks abscess formation, Proc. Natl. Acad. Sci. USA 102 (2005) 1691–1696.

[34] Nakayama J., Chen S., Oyama N., Nishiguchi K., Azab E.A., Tanaka E., Kariyama R., Sonomoto K., Revised model for *Enterococcus faecalis fsr* quorum-sensing system: the small open reading frame *fsrD* encodes the gelatinase biosynthesis-activating pheromone propeptide corresponding to staphylococcal AgrD, J. Bacteriol. 188 (2006) 8321–8326.

Appendix A: Nondimensionalisation and initial conditions

For Models I and II we employ the same nondimensionalisations in order to make easier comparisons. Due to the extra variables in Model III we need to adapt the nondimensionalisation so that it is as consistent as possible with the first two.

We start by describing the totally down-regulated steady states of the three models. This is what would arise if no AIP were produced ($k = 0$) and no inhibitor molecules are present ($k_i = 0$), so that QS has absolutely no effects. For Model I these are given by

$$\begin{aligned}
&\tilde{M} = \frac{Nm}{\delta_M}, && \tilde{A} = \frac{N\kappa m}{\delta_M \delta_A}, && \tilde{a}, \tilde{R_P^*}, \tilde{A_P}, \tilde{P}, \tilde{i}, \tilde{R^i} = 0, \\
&\tilde{B} = \frac{N\kappa m}{\delta_M(\alpha_T + \delta_B)}, && \tilde{C} = \frac{N\kappa m}{\delta_M(\alpha_R + \delta_C)}, && \tilde{D} = \frac{N\kappa m}{\delta_M(\alpha_S + \delta_D)}, \\
&\tilde{T} = \frac{N\alpha_T\kappa m}{\delta_M\delta_T(\alpha_T + \delta_B)}, && \tilde{R} = \frac{N\alpha_R\kappa m}{\delta_M\delta_R(\alpha_R + \delta_C)}, && \tilde{S} = \frac{N\alpha_S\kappa m}{\delta_M\delta_S(\alpha_S + \delta_D)},
\end{aligned} \tag{22}$$

where $\tilde{X}$ denotes the completely down-regulated steady state of variable X, i.e. where protein levels are directed only by basal mRNA transcription and not by *agr*-induced transcription. It is important to remember that these are not the steady states of a system where inhibitor molecules have suppressed the *agr* operon.

Those which change for Model II are

$$\begin{aligned}
\tilde{A} =& \frac{N\kappa m(\mu + \delta_{A_P})}{\delta_M((\psi_A + \delta_A)(\mu + \delta_{A_P}) - \psi_A\mu)}, \quad \tilde{A_P} = \frac{N\psi_A\kappa m}{\delta_M((\psi_A + \delta_A)(\mu + \delta_{A_P}) - \psi_A\mu)}, \\
&\tilde{P} = \frac{b\kappa m(\mu + \delta_{A_P})}{b\kappa m(\mu + \delta_{A_P}) + u\delta_M((\psi_A + \delta_A)(\mu + \delta_{A_P}) - \psi_A\mu)}.
\end{aligned} \tag{23}$$

Those which differ from (22) for Model III are

$$\tilde{R} = \frac{N\alpha_R\kappa m}{\delta_M(\alpha_R + \delta_C)(\psi_R + \delta_R)}, \quad \tilde{R_P} = \frac{N\psi_R\alpha_R\kappa m}{\delta_M\delta_{R_P}(\alpha_R + \delta_C)(\psi_R + \delta_R)}, \quad \tilde{R^*}, \tilde{R_P^i} = 0. \tag{24}$$

Models I and II

We now use (22) to nondimensionalise the relevant variables (namely mRNA and all unphosphorylated proteins, with the exception of phosphorylated AgrA in Model II, since these are the only species present in a totally down-regulated cell). Hence we set

$$M' = \frac{\delta_M}{Nm}M, \qquad A' = \frac{\delta_M\delta_A}{N\kappa m}A, \qquad X' = \frac{\delta_M(\alpha_Y + \delta_X)}{N\kappa m}X, \qquad Y' = \frac{\delta_M\delta_Y(\alpha_Y) + \delta_X}{N\alpha_Y\kappa m}Y, \tag{25}$$

for $X = B, C, D$ and $Y = T, R, S$ respectively. The remaining nondimensionalisations are chosen to simplify the corresponding equations as much as possible, namely to set the coefficients of basal mRNA transcription, AIP-receptor binding, AgrA activation and phosphorylated AgrA binding to the promoter site in certain equations to unity. They are

given by

$$\begin{aligned} a' &= \frac{\beta\phi b N \alpha_R \kappa^2 m^2}{{\delta_M}^5 \delta_A \delta_R(\alpha_R+\delta_C)} a, \quad {R_P^*}' = \frac{\phi b \kappa m}{{\delta_M}^3 \delta_A} R_P^*, \qquad {A_P}' = \frac{b}{N\delta_M} A_P, \\ i' &= \frac{\beta_i \gamma_i}{{\delta_M}^2} i, \qquad\qquad {R^i}' = \frac{\gamma_i \delta_R(\alpha_R+\delta_C)}{N\alpha_R\kappa m} R^i, \quad \tau = \delta_M t, \end{aligned} \tag{26}$$

P already being dimensionless. Time is thus scaled with δ_M, the rate of mRNA degradation. Dimensionless parameters are introduced according to

$$\lambda'_X = \frac{\delta_X}{\delta_M} \quad \text{for} \quad X = A, T, R, S, R_P^*, A_P, i, R^i, \tag{27}$$

$$\alpha'_{X,Y} = \frac{\alpha_Y + \delta_X}{\delta_M} \quad \text{for} \quad (X,Y) = (B,T), (C,R) \text{ or } (D,S), \tag{28}$$

and

$$\begin{aligned} &\lambda_a = \frac{\lambda_a}{\delta_M}, \quad v' = \frac{v}{m}, \quad \beta' = \frac{\beta\tilde{R}}{\delta_M}, \quad {\beta_i}' = \frac{\beta_i \tilde{R}}{\delta_M}, \quad \eta = \frac{N\beta\delta_M}{\phi b \tilde{A}}, \quad \gamma' = \frac{\gamma}{\delta_M}, \quad {\gamma_i}' = \frac{\gamma_i}{\delta_M}, \\ &k_S = \frac{k\tilde{T}}{\delta_M}, \quad u' = \frac{u}{\delta_M}, \quad \mu' = \frac{\mu}{\delta_M}, \quad \phi' = \frac{N\delta_M}{b\tilde{A}}, \quad {k_i}' = \frac{\beta_i\gamma_i k_i}{{\delta_M}^3}, \quad k_a = \frac{k\beta\phi b \tilde{A}\tilde{T}\tilde{R}\tilde{S}}{N{\delta_M}^4}, \quad {\psi_A}' = \frac{\psi_A}{\delta_M}, \end{aligned} \tag{29}$$

where $\tilde{X}$ is the initial condition of X given by (22), for $X = A, T, R, S$.

We assume that protein degradation rates are negligible in comparison to the dilution rate so, since $\delta_X = \lambda_X + r$ we set all the parameters in (27) to be equal. By additionally assuming that AgrB and AgrC are taken into the membrane at the same rate and that AgrD is anchored at this same rate, we can do the same in (28). Thus we take

$$\begin{aligned} \lambda'_X &= \lambda \quad \text{for} \quad X = A, T, R, S, R_P^*, A_P, \\ \alpha'_{X,Y} &= \alpha \quad \text{for} \quad (X,Y) = (B,T), (C,R) \text{ or } (D,S). \end{aligned} \tag{30}$$

Dropping $'$'s we get the nondimensional models represented by Figures 6 and 7. The initial conditions are given by the dimensionless natural down-regulated steady state which for Model I is simply

$$\begin{aligned} M(0) = A(0) = B(0) = C(0) = D(0) = S(0) = T(0) = R(0) = 1, \\ a(0) = R^*(0) = A_P(0) = P(0) = 0. \end{aligned} \tag{31}$$

Those which change for Model II are

$$A(0) = \frac{\mu+\lambda}{\mu+\lambda+\psi_A}, \quad A_P(0) = \frac{\psi_A}{(\mu+\lambda+\psi_A)\phi}, \quad P(0) = \frac{\phi}{\phi + ub\lambda(\mu+\lambda)((\psi_A+\lambda)(\mu+\lambda) - \psi_A\mu)}, \tag{32}$$

and differ because constitutive AgrA phosphorylation means both A and A_P will be present in a down-regulated cell and some induction of the operon will occur (making P non-zero also in a down-regulated state) in response to the (presumably low) levels of AgrA. These are used as initial conditions in the numerical simulations illustrated by Figures 12(a) and 13(a).

Model III

We nondimensionalise the relevant variables using the down-regulated steady states of this model (rather than those of Model I) and choose the remaining nondimensionalisations to ensure the equivalent terms have coefficient unity as in the previous two models.

The nondimensional variables which alter from (25) and (26) are

$$\begin{aligned} R' &= \frac{\delta_M(\alpha_R+\delta_C)(\psi_R+\delta_R)}{N\alpha_R\kappa m}R, \quad {R_P}' = \frac{\delta_M\delta_{R_P}(\alpha_R+\delta_C)(\psi_R+\delta_R)}{N\psi_R\alpha_R\kappa m}R_P, \quad {R^*}' = \frac{b}{N\delta_M}R^*, \\ a' &= \frac{\beta\phi bN\alpha_R\kappa^2m^2}{{\delta_M}^5\delta_A(\alpha_R+\delta_C)(\psi_R+\delta_R)}a, \quad {R_P^i}' = \frac{\gamma_i\delta_{R_P}(\alpha_R+\delta_C)(\psi_R+\delta_R)}{N\psi_R\alpha_R\kappa m}R_P^i. \end{aligned} \tag{33}$$

The nondimensional parameters which differ from (27)-(30) are

$$\begin{aligned} {\lambda_X}' &= \frac{\delta_X}{\delta_M} = \lambda \quad \text{for} \quad X = A, T, R, S, R_P, R_P^*, R^*, R_P^i, A_P, a, i, \\ {\psi_R}' &= \frac{\psi_R}{\delta_M}, \quad k_a = \frac{k\beta\phi b\tilde{A}\tilde{T}\tilde{R}_P\tilde{S}}{N{\delta_M}^4}, \quad \beta' = \frac{\beta\tilde{R}_P}{\delta_M}, \quad {\beta_i}' = \frac{\beta_i\tilde{R}_P}{\delta_M}, \quad \zeta = \frac{b\tilde{R}_P}{N\delta_M}. \end{aligned} \tag{34}$$

Dropping $'$'s the resulting nondimensional model is illustrated by Figure 8. The initial conditions (again, the nondimensional natural down-regulated steady states) which change from (31) (i.e. Model I) are

$$R_P(0) = 1 \quad \text{and} \quad R^*(0), R_P^i(0) = 0. \tag{35}$$

These are used as initial conditions in Figure 14(a).

Appendix B: Derivation of the asymptotic approximations

We here describe the derivation of our asymptotic approximations (introduced in §3 and given explicitly in §4) to the steady-state curves of Figure 9. In each case, the appropriate scalings of k_i are chosen in order to capture the requisite information from the asymptotic analysis in order to represent each section of the curve. These (distinguished-limit) scalings reflect how sensitive each TCS cascade is to inhibitor therapy and are provided in Table 4. We recall that our small parameter ϵ represents the ratio of the rate of basal mRNA transcription to that of QS-controlled transcription. Notice that considerably larger scalings of k_i are required in Model I due to the fact that it is the least susceptible to inhibition of the three models.

For each model we obtain two sets of scalings which cover the full solution curve: one represents both the active stable branch and the unstable branch, while the other incorporates the inactive stable branch and the lower fold bifurcation; in each case there is, in the usual way, an intermediate regime in which the two approximations overlap (i.e. furnish the same solutions at leading order) and we also derive these regimes here. The scalings of k_i and each variable needed to

	Model I scaling		Model II scaling		Model III scaling	
	Active	Inactive	Active	Inactive	Active	Inactive
k_i	$\frac{1}{\epsilon^6}k_i^\dagger$	$\frac{1}{\epsilon^3}k_i^\ddagger$	$\frac{1}{\epsilon^4}k_i^\dagger$	$\frac{1}{\epsilon}k_i^\ddagger$	$\frac{1}{\epsilon^4}k_i^\dagger$	$\frac{1}{\epsilon^2}k_i^\ddagger$
P	$\hat{P}^\dagger$	$\epsilon P^\ddagger$	$\hat{P}^\dagger$	$\epsilon P^\ddagger$	$\hat{P}^\dagger$	$\epsilon P^\ddagger$
M	$\frac{1}{\epsilon}M^\dagger$	$M^\ddagger$	$\frac{1}{\epsilon}M^\dagger$	$M^\ddagger$	$\frac{1}{\epsilon}M^\dagger$	$M^\ddagger$
R_P^*	$\epsilon {R_P^*}^\dagger$	$\epsilon {R_P^*}^\ddagger$	$\frac{1}{\epsilon}{R_P^*}^\dagger$	$\frac{1}{\epsilon}{R_P^*}^\ddagger$	$\epsilon {R_P^*}^\dagger$	$\epsilon {R_P^*}^\ddagger$
A_P	$A_P^\dagger$	$\epsilon A_P^\ddagger$	$\frac{1}{\epsilon}A_P^\dagger$	$A_P^\ddagger$	$A_P^\dagger$	$\epsilon A_P^\ddagger$
A	$\frac{1}{\epsilon}A^\dagger$	$A^\ddagger$	$A^\dagger$	$\epsilon A^\ddagger$	$\frac{1}{\epsilon}A^\dagger$	$A^\ddagger$
R	$\epsilon^5 R^\dagger$	$\epsilon^3 R^\ddagger$	$\epsilon^3 R^\dagger$	$\epsilon R^\ddagger$	$\frac{1}{\epsilon}R^\dagger$	$R^\ddagger$
a	$\frac{1}{\epsilon^4}a^\dagger$	$\frac{1}{\epsilon^2}a^\ddagger$	$\frac{1}{\epsilon^4}a^\dagger$	$\frac{1}{\epsilon^2}a^\ddagger$	$\frac{1}{\epsilon^4}a^\dagger$	$\frac{1}{\epsilon^2}a^\ddagger$
i	$\frac{1}{\epsilon^6}i^\dagger$	$\frac{1}{\epsilon^3}i^\ddagger$	$\frac{1}{\epsilon^4}i^\dagger$	$\frac{1}{\epsilon}i^\ddagger$	$\frac{1}{\epsilon^4}i^\dagger$	$\frac{1}{\epsilon^2}i^\ddagger$
R_P	-	-	-	-	$\epsilon^3 \hat{R}_P^\dagger$	$\epsilon^2 R_P^\ddagger$
R^*	-	-	-	-	${R^*}^\dagger$	$\epsilon {R^*}^\ddagger$

Table 4: The distinguished scalings required for the asymptotic approximation to the active and inactive sections of the solution curves illustrated in Figure 9 (the former also incorporate the unstable branch). The scalings required for $B(\tau), C(\tau), D(\tau), S(\tau), T(\tau), R^i(\tau)$ and $R_P^i(\tau)$ are the same as those given for $M(\tau)$. The variables R_P and R^* appear in Model III only.

produce the asymptotic approximation to the active and unstable branches are denoted by $X^\dagger$; when they are scaled to approximate the inactive branch we use $X^\ddagger$. The steady state approximations for each variable X are denoted $\bar{X}^\dagger$ and $\bar{X}^\ddagger$. Since, in the steady state, $\bar{M} \equiv \bar{B} \equiv \bar{C} \equiv \bar{D} \equiv \bar{T}$ (mRNA concentration and natural degradation, which we have assumed to occur at the same rate for all proteins, are the only reactions influencing the levels of these proteins), we eliminate B, C, D and T in favour of M in the remainder of this appendix.

Model I

Active stable branch and unstable branch

Substituting the scalings from Table 4 into Model I (given in Figure 6) we obtain the following steady-state equations:

$$0 = A_P^\dagger(1 - P^\dagger) - uP^\dagger, \tag{36}$$

$$0 = \hat{v}P^\dagger - M^\dagger + \epsilon, \tag{37}$$

$$0 = \lambda(M^\dagger - S^\dagger) - \hat{k}_S M^\dagger S^\dagger, \tag{38}$$

$$0 = \lambda(M^\dagger - A^\dagger) - \epsilon\phi A^\dagger {R_P^*}^\dagger + \epsilon^2\hat{\mu}\phi A_P^\dagger, \tag{39}$$

$$0 = A^\dagger {R_P^*}^\dagger - (\lambda + \epsilon\hat{\mu})A_P^\dagger, \tag{40}$$

$$0 = \hat{k}_a M^\dagger S^\dagger - \epsilon^4\hat{\beta}R^\dagger a^\dagger + \epsilon^4\hat{\beta}\gamma {R_P^*}^\dagger - \lambda_a a^\dagger, \tag{41}$$

$$0 = k_i^\dagger - \epsilon^4\hat{\beta}_i R^\dagger i^\dagger + \epsilon^4\hat{\beta}_i\gamma_i {R^i}^\dagger - \lambda_i i^\dagger, \tag{42}$$

$$0 = R^\dagger a^\dagger - (\lambda + \gamma){R_P^*}^\dagger, \tag{43}$$

$$0 = R^\dagger i^\dagger - (\lambda + \gamma_i){R^i}^\dagger, \tag{44}$$

$$0 = \lambda M^\dagger - \epsilon^6\lambda R^\dagger - \epsilon^3\frac{\eta}{\hat{\beta}}R^\dagger a^\dagger + \epsilon^3\frac{\eta\gamma}{\hat{\beta}}{R_P^*}^\dagger - \frac{1}{\gamma_i}R^\dagger i^\dagger + {R^i}^\dagger. \tag{45}$$

The leading-order balances of (36)-(45) (i.e. those in which all terms involving ϵ are neglected) can be solved to obtain (8) and (9).

Inactive branch

Using the scalings from Table 4 we derive the steady-state equations to represent the stable branch which represents inactive cells. Equations (39),(40),(43) and (44) also hold for this branch; the equations which change are

$$0 = A_P^\ddagger(1 - \epsilon P^\ddagger) - uP^\ddagger, \tag{46}$$

$$0 = \hat{v}P^\ddagger - M^\ddagger + 1, \tag{47}$$

$$0 = \lambda(M^\ddagger - S^\ddagger) - \epsilon\hat{k}_S M^\ddagger S^\ddagger, \tag{48}$$

$$0 = \hat{k}_a M^\ddagger S^\ddagger - \epsilon^2\hat{\beta}R^\ddagger a^\ddagger + \epsilon^2\hat{\beta}\gamma {R_P^*}^\ddagger - \lambda_a a^\ddagger, \tag{49}$$

$$0 = k_i^\ddagger - \epsilon^2\hat{\beta}_i R^\ddagger i^\ddagger + \epsilon^2\hat{\beta}_i\gamma_i {R^i}^\ddagger - \lambda_i i^\ddagger, \tag{50}$$

$$0 = \lambda M^\ddagger - \epsilon^3\lambda R^\ddagger - \epsilon^2\frac{\eta}{\hat{\beta}}R^\ddagger a^\ddagger + \epsilon^2\frac{\eta}{\hat{\beta}}\gamma {R_P^*}^\ddagger - \frac{1}{\gamma_i}R^\ddagger i^\ddagger + {R^i}^\ddagger. \tag{51}$$

Solving the leading-order terms of (39),(40),(43),(44) and (46)-(51) gives us the asymptotic approximations on the inactive stable branch, i.e. (10) and (11). We note that the 'near-field' limit ($k_i^\dagger \to 0$) of (9) and the 'far-field' one ($k_i^\ddagger \to \infty$)

of (11) are

$$\bar{P}^\dagger \sim \bar{P}^\ddagger \sim \left(\frac{(\lambda+\gamma)\lambda\lambda_a u}{(\lambda+\gamma_i)\lambda_i\gamma_i\hat{v}^4\hat{k}_a}\right)^{\frac{1}{3}} {k_i^\dagger}^{\frac{1}{3}},$$

(where $k_i^\dagger = k_i^\ddagger$), i.e. this describes the intermediate region in which the two approximations each hold.

Model II

Active stable branch and unstable branch

Using the scalings provided in Table 4, we find that equations (37),(38),(43) and (44) also apply to Model II. Those equations that differ are,

$$0 = \frac{1}{\phi}A^\dagger(1-P^\dagger) - uP^\dagger, \quad (52) \qquad 0 = \hat{k}_a M^\dagger S^\dagger - \epsilon^2\hat{\beta}R^\dagger a^\dagger + \epsilon^2\hat{\beta}\gamma {R_P^*}^\dagger - \lambda_a a^\dagger, \quad (54)$$

$$0 = \frac{\hat{\psi}_A}{\phi}A^\dagger - \phi A_P^\dagger {R_P^*}^\dagger - (\lambda+\epsilon\hat{\mu})A_P^\dagger, \quad (53) \qquad 0 = k_i^\dagger - \epsilon^2\hat{\beta}_i R^\dagger i^\dagger + \epsilon^2\hat{\beta}_i\gamma_i {R^i}^\dagger - \lambda_i i^\dagger, \quad (55)$$

$$0 = \epsilon\lambda M^\dagger - \epsilon^2\lambda A^\dagger - \hat{\psi}_A A^\dagger + \phi^2 A_P^\dagger {R_P^*}^\dagger + \epsilon^2\hat{\mu}\phi A_P^\dagger, \quad (56)$$

$$0 = \lambda M^\dagger - \epsilon^4\lambda R^\dagger - \epsilon\frac{\eta}{\hat{\beta}}R^\dagger a^\dagger + \epsilon\frac{\eta\gamma}{\hat{\beta}}{R_P^*}^\dagger - \frac{1}{\gamma_i}R^\dagger i^\dagger + {R^i}^\dagger. \quad (57)$$

We manipulate the leading-order terms to obtain the approximations to the active and unstable branches of the solution curves, i.e. (12) and (13).

Inactive branch

For the inactive branch we again find that some of the steady state equations do not alter from Model I, namely (43), (44), (47), and (48). The remaining equations are given by

$$0 = \frac{1}{\phi}A^\ddagger(1-\epsilon P^\ddagger) - uP^\ddagger, \quad (58) \qquad 0 = \hat{k}_a M^\ddagger S^\ddagger - \hat{\beta}R^\ddagger a^\ddagger + \hat{\beta}\gamma {R_P^*}^\ddagger - \lambda_a a^\ddagger, \quad (60)$$

$$0 = \epsilon\frac{\hat{\psi}_A}{\phi}A^\ddagger - \phi A_P^\ddagger {R_P^*}^\ddagger - (\lambda+\epsilon\hat{\mu})A_P^\ddagger, \quad (59) \qquad 0 = k_i^\ddagger - \hat{\beta}_i R^\ddagger i^\ddagger + \hat{\beta}_i\gamma_i {R^i}^\ddagger - \lambda_i i^\ddagger, \quad (61)$$

$$0 = \epsilon\lambda M^\ddagger - \epsilon^2\lambda A^\ddagger - \hat{\psi}_A A^\ddagger + \phi^2 A_P^\ddagger {R_P^*}^\ddagger + \epsilon^2\hat{\mu}\phi A_P^\ddagger, \quad (62)$$

$$0 = \lambda M^\ddagger - \epsilon\lambda R^\ddagger - \frac{\eta}{\hat{\beta}}R^\ddagger a^\ddagger + \frac{\eta\gamma}{\hat{\beta}}{R_P^*}^\ddagger - \frac{1}{\gamma_i}R^\ddagger i^\ddagger + {R^i}^\ddagger. \quad (63)$$

The leading-order terms of these equations allow us to calculate the approximations to the inactive stable branch, i.e. (14)-(16). The region where both (13) and this approximation to the inactive branch hold, i.e. $k_i^\dagger \to 0$ and $k_i^\ddagger \to \infty$, is given by

$$\bar{P}^\dagger \sim \bar{P}^\ddagger \sim \left(\frac{(\lambda+\gamma)\lambda_a u\hat{\psi}_A}{(\lambda+\gamma_i)\lambda_i\gamma_i\hat{k}_a\hat{v}^4}\right)^{\frac{1}{3}} {k_i^\dagger}^{\frac{1}{3}}.$$

Model III

Active stable branch and unstable branch

We have that (36) and (38)-(40) all also hold for Model III. In addition we have

$$0 = (\lambda + \psi_R)(M^\dagger - R^\dagger) + \epsilon \frac{\gamma \psi_R}{\lambda \zeta} R^{*\dagger}, \tag{64}$$

$$0 = R_P^\dagger a^\dagger - \frac{\hat{\beta}}{\eta \zeta} A^\dagger R_P^{*\dagger} - \epsilon^2 (\lambda + \gamma) R_P^{*\dagger}, \tag{65}$$

$$0 = A^\dagger R_P^{*\dagger} - (\lambda + \gamma) R^{*\dagger}, \tag{66}$$

$$0 = R_P^\dagger i^\dagger - (\lambda + \gamma_i) R_P^{i\,\dagger}, \tag{67}$$

$$0 = k_i^\dagger - \epsilon^2 \hat{\beta}_i R_P^\dagger i^\dagger + \epsilon^2 \hat{\beta}_i \gamma_i R_P^{i\,\dagger} - \lambda_i i^\dagger, \tag{68}$$

$$0 = \lambda R^\dagger - \epsilon^4 \lambda R_P^\dagger - \epsilon \frac{\eta}{\hat{\beta}} R_P^\dagger a^\dagger + \epsilon^3 \frac{\eta \gamma}{\hat{\beta}} R_P^{*\dagger} - \frac{1}{\gamma_i} R_P^\dagger i^\dagger + R_P^{i\,\dagger}, \tag{69}$$

$$0 = \hat{k}_a M^\dagger S^\dagger - \epsilon^2 \hat{\beta} R_P^\dagger a^\dagger + \epsilon^4 \hat{\beta} \gamma R_P^{*\dagger} + \epsilon^2 \frac{\hat{\beta}^2 \gamma}{\eta \zeta} R^{*\dagger} - \lambda_a a^\dagger. \tag{70}$$

The dominant terms give (17) and (18), i.e. the asymptotic approximations to the active stable and unstable branches for Model III.

Inactive branch

Equations (39), (40) and (46)-(48) all also apply for this model. Those which differ are

$$0 = (\lambda + \psi_R)(M^\ddagger - R^\ddagger) + \epsilon \frac{\gamma \psi_R}{\lambda \zeta} R^{*\ddagger}, \tag{71}$$

$$0 = R_P^\ddagger a^\ddagger - \frac{\hat{\beta}}{\eta \zeta} A^\ddagger R_P^{*\ddagger} - \epsilon (\lambda + \gamma) R_P^{*\ddagger}, \tag{72}$$

$$0 = A^\ddagger R_P^{*\ddagger} - (\lambda + \gamma) R^{*\ddagger}, \tag{73}$$

$$0 = R_P^\ddagger i^\ddagger - (\lambda + \gamma_i) R_P^{i\,\ddagger}, \tag{74}$$

$$0 = k_i^\ddagger - \epsilon \hat{\beta}_i R_P^\ddagger i^\ddagger + \epsilon \hat{\beta}_i \gamma_i R_P^{i\,\ddagger} - \lambda_i i^\ddagger, \tag{75}$$

$$0 = \lambda R^\ddagger - \epsilon^2 \lambda R_P^\ddagger - \epsilon \frac{\eta}{\hat{\beta}} R_P^\ddagger a^\ddagger + \epsilon^2 \frac{\eta \gamma}{\hat{\beta}} R_P^{*\ddagger} - \frac{1}{\gamma_i} R_P^\ddagger i^\ddagger + R_P^{i\,\ddagger}, \tag{76}$$

$$0 = \hat{k}_a M^\ddagger S^\ddagger - \epsilon \hat{\beta} R_P^\ddagger a^\ddagger + \epsilon^2 \hat{\beta} \gamma R_P^* + \epsilon \frac{\hat{\beta}^2 \gamma}{\eta \zeta} R^{*\ddagger} - \lambda_a a^\ddagger. \tag{77}$$

As before, the leading-order terms can be rearranged to give (19) and (20). The intermediate region in which (18) and (20) each hold, i.e. $k_i^\dagger \to 0$ and $k_i^\ddagger \to \infty$, is given by

$$\bar{P}^\dagger \sim \bar{P}^\ddagger \sim \left(\frac{\lambda \lambda_a u \hat{\beta}}{(\lambda + \gamma_i) \lambda_i \gamma_i \eta \zeta \hat{k}_a \hat{v}^3} \right)^{\frac{1}{2}} k_i^{\dagger\,\frac{1}{2}}.$$

List of Figures

List of Tables